ISSN 1061-3862, International Journal of Self-Propagating High-Temperature Synthesis, 2024, Vol. 33, No. 1, pp. 1–25. © Allerton Press, Inc., 2024.

Self-Propagating High-Temperature Synthesis of Complex Phases: The Example of TiC-Based Composites

W. Ramdane*

Department of Physics, Faculty of Sciences, University of 20 August 1955-Skikda, BP 26, Road d'El-Hadaiek, Skikda, 21000 Algeria

**e-mail: rwisseme@yahoo.fr*

Received February 27, 2023; revised July 20, 2023; accepted September 15, 2023

Abstract—TiC-based composites with various initial compositions can be successfully synthesized by self-propagating high-temperature synthesis (SHS) from either mixtures containing thermite reactions or from pure elements. The effect of various experimental parameters on the combustion reaction kinetics and the relationship between structure, microstructure and mechanical behavior of products was identified. It was found that the matrix's strengthening is one of the most important variables in boosting the composite's strength, and adding alloy elements reduces the rate and size of cracks and pores in the cermet microstructure. The presence of TiC particles inhibits dislocation motion and has a significant effect on the composite's mechanical behavior.

Keywords: self-propagating high-temperature synthesis (SHS), TiC-based composites, cermets, thermite reactions, sintering additives, mechanical properties, formation mechanisms

DOI: 10.3103/S1061386224010059

1. INTRODUCTION

Metal matrix composites (MMCs) are an exciting area of research, improving properties of elastic modulus, wear resistance, and strength of unreinforced metals and alloys [1, 2], as well as, titanium carbide (TiC) matrix composites receive constantly great attention because of their excellent hardness [3, 4], high flexural strength [4, 5], high thermal conductivity [4, 6], and extreme thermal [4, 5] and erosion stability [4, 7]. TiC is progressively used as reinforcing particles in composites due to its excellent performance, such as high melting point, high modulus, high hardness, high conductivity, low density [8, 9], excellent high-temperature strength [10, 11], thermal [12, 13] and mechanical stability [14, 15], excellent thermal shock and ablation resistance [5, 16]. Thus, according to the famous inherent characteristics, TiC matrix composites are considered a material of choice in many areas, such as cutting tools [4, 17], rocket nozzles [4, 9], and others [4].

It is confirmed that TiC is considered as an ideal candidate to strengthen the tungsten matrix [10, 11]. Then the addition of TiC can play an active role in improving the comprehensive properties of tungsten matrix composites [20] As well TiC is one of the popular reinforcing phases for iron matrix [12, 13]. The utility of adding TiC as a reinforcement element is explored by many works. Results showed that higher relative content of TiC can significantly enhance the electrical conductivity of Si/TiC–SiC/C composites [15]. In another study, the increase in the fracture toughness of NiAl by adding ceramic phases is confirmed by reference [21]. Researchers found that the ceramic reinforcement of $2TiB_2 + TiC$ is more effective than that of $TiB_2 + 2TiN$ [21]. Adding that in ceramic matrix composites, TiC as reinforcing material exhibits large elastic modulus induced by its unique structure of the metal-like carbides, thus compensating for higher toughness of the ZrO_2 [22, 23]. Among the carbides of transition metals, TiC has the highest room temperature hardness. TiC is one of the most wear-resistant materials used at room temperature [24, 25] However, the hardness of TiC decreases sharply with the increase in the temperature. TiC–TiB_2 composite ceramics have been prepared in recent years due to the excellent plastic deformation resistance of TiB_2 at high temperature and compared to single-phase TiC and TiB_2 ceramic materials, the hardness of composite ceramic materials containing TiC and TiB_2 is increased greatly [25, 26].

The size, distribution, and morphology of TiC particles have a great influence on the mechanical properties of final composites. Reference [8] reported the combustion synthesis and hot-pressing of TiC/Fe composites in the Fe–Ti–C system with different carbon source and molar ratio. The results showed that the size of TiC particles decreases with increase of Fe content in Fe–Ti–C systems produced by the same carbon source, while the particles change from spher-

ical shapes to cubic shapes which can reduce stress concentration between the ceramic particles and the matrix [8]. Reference [27] investigated that the Fe particles in the thermal explosion of Fe-TiC composite layers on a steel substrate lead to a lack of exothermic heat for the completion of the reaction. Even in case of incomplete reactions, the distribution of hard particles in the iron matrix can improve the overall hardness of the sheath layer [27]. A notable TiC particle coarsening was induced by the Cr addition in the thermal explosion synthesis of TiC–Ni-based cermets, but adding Mo or W inhibited the grain growth and the final cermet had a lower relative density. The highest hardness value (18000 MPa) was recorded for TiC–Ni cermet containing Mo. Hardness was 16320 MPa and 15110 MPa for cermets with W and Cr additions, respectively [28].

In another study, the reduction in the mechanical properties of TiC–Al cermets at room temperature after adding 5 vol % Nb and 5 vol % Zr elements produced by combustion synthesis and hot-pressing method, respectively, was due to the presence of intermediate phases and TiC grain refinement. Crystal mismatch at the Al–TiC interface improved the mechanical properties of final products [29], and the increase of TiC content, the hardness of cermets gradually increased as demonstrated by Hongwei Zhao and Jinhong Li in their work [30].

Another way to produce TiC-based composites is SHS involving thermite reactions. Thermite reactions play an important role in their reactive performance [31] and then for this reason, termites have become the focus of much research on the synthesis of materials and composites by several methods of elaboration. In this regard, Pavel A. Miloserdov and Vladimir A. Gorshkov [32] reported the metallothermic SHS of Al_2O_3–Cr_2O_3 ceramic reinforced with TiC particles from mixture containing 80–85% (TiO_2 + Al + C) and 20–15% (CrO_3 + Al) in order to prepare materials promising for use as tools in the machining high-strength steels with a hardness of up to 49 HRC. They showed that Al_2O_3–Cr_2O_3 + TiC final ceramic composite is colored bright red typical of ruby. This indicated that the Cr_2O_3 content in Al_2O_3 is more than 6%. They also found that Al_2O_3–Cr_2O_3 + TiC composite after 24-h milling followed by pressing and sintering is very dense and has density of 4.55 g/cm^3, hardness of 20 GPa, flexural strength of 680 MPa, and crack resistance of 4.2 MPa m$^{1/2}$ [32].

In this brief review, we studied the self-propagating high-temperature synthesis of TiC-based composites including the influence of using thermite reactions on the combustion process. The effect of mechanical activation before combustion synthesis, particle size of raw powders, stoichiometry, and additives was investigated, in terms of the combustion reaction kinetics, ignition and adiabatic temperatures, phase composition of final samples and formation mechanism of TiC-based composites. The relationship between structure, microstructure, and mechanical properties of final SHS products was presented.

2. COMBUSTION SYNTHESIS OF TiC-BASED COMPOSITES INVOLVING THERMITE REACTIONS

The SHS reactions involving aluminothermic reduction of metal oxides were greatly used to produce TiC-based composites [31]. In this topic, the synthesis of TiC–MgO composite according to the reaction (1) $TiO_2 + 2Mg + C = TiC + 2MgO$ can be viewed as the sum of two sequential reactions, the first is a thermite reaction in which titanium oxide is reduced by the metal and the second involves the reaction between titanium and carbon, consequently the product of reaction (1) is multiphase [33]. Reactions such as Eq. (1) include highly exothermic thermite reactions and thus are associated with high adiabatic temperatures, as a result the formation of products occurs in the liquid phase [33].

A large number of investigations on the use of thermite reactions and SHS process to prepare TiC-based composites have been reported such as:

$$3TiO_2 + 3C + (4 + x)\,Al = 3TiC + 2Al_2O_3 + x\,Al \ [34, 35], \quad (2)$$

$$3TiO_2 + 4Al + 3C + x\,Fe = 3TiC + 2Al_2O_3 + x\,Fe \ [36, 37], \quad (3)$$

$$5Al + 3NiO + Ti + C = 3NiAl + Al_2O_3 + TiC \ [38], \quad (4)$$

$$2Al + 3NiO + Ti + C = 3Ni + Al_2O_3 + TiC \ [39], \quad (5)$$

$$TiO_2 + C + 2Mg = TiC + 2MgO \ [40], \quad (6)$$

$$3TiO_2 + 3C + 4Al = 3TiC + 2Al_2O_3 \ [40]. \quad (7)$$

When the aim of the study is the production of a specific material, thermites are used to produce some additional energy to favor a particular synthesis reaction [41]. For example, in the case where the thermite mixture surrounds the sample, it is only its exothermic aspect that is interesting, and therefore there is no interaction between the sample and the thermite blend [41] as seen in Fig. 1. Such an approach was demonstrated by the authors of [42]. They used the highly exothermic thermite reaction (8) $Fe_2O_3 + 2Al = 2Fe + Al_2O_3$ as a match to ignite another reaction (Ti + C) to form TiC. Reference [42] reported that the addition of alumina (Al_2O_3) as diluent is used to avoid explosion of materials. As for the other case where the thermite powders mixed with the other reactants, in that case, it is difficult to separate the products of the thermite reaction from the others [41] and the interest in these composites is focused on their intrinsic properties [33]. For example, the self-propagating high-tem-

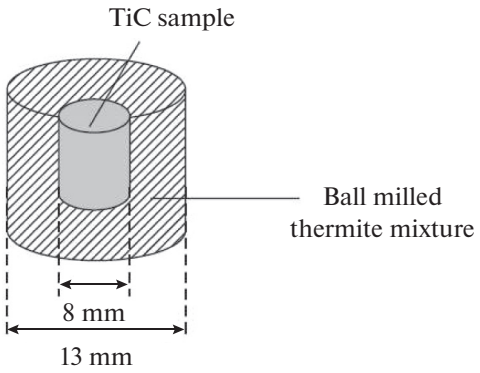

Fig. 1. Ti–C sample surounded by a ball-milled thermite mixture [42].

perature synthesis of TiC–Ni–Al_2O_3 cermet presented by reference [39] (Fig. 2). The authors used Ni addition to the (Ti + C) powders as the result of the aluminothermic reduction of NiO according to the reaction (9) $3NiO + 2Al = 3Ni + 2Al_2O_3$. After (3NiO + 2Al) addition, reactions were highly exothermic and propagated rapidly through the raw samples. They found that the use of 5 and 10% of Al_2O_3 as a diluent slows down the reaction and the combusted pellets are not fractured. Alumina does not cause the extinction of the combustion front and the morphologies of all samples with additives are characterized by a lamellar structure (Fig. 3) [39]. We can add the aluminothermic reaction

$$7 \times 73Al + Co_2O_3 + Cr_2O_3 + Fe_2O_3 + 2NiO \rightarrow 3 \times 66Al_2O_3 + 2CoCrFeNiAl_{0.2}, \quad (10)$$

studied by Guannan Zhang and Xiao Yang [43]. They used this reaction to produce $CoCrFeNiAl_{0.2}(TiC)_x$ ($x = 0$, 0.06, 0.12, and 0.20) by high-gravity combustion synthesis (HGCS). $CoCrFeNiAl_{0.2}$ high-entropy alloys (HEAs) were obtained by inducing a thermic reaction between the several low-cost metal oxides (Co_2O_3, Cr_2O_3, Fe_2O_3, NiO) and Al powders. Then Ti reacts with C to form TiC followed by the dissolution and precipitation principle. The in-situ synthesized TiC and the small amount of BCC phase are accompanied by enhancing the compressive strength, bending strength, and hardness of composites by refining the grain of HEAs [43].

3. THE IGNITION BEHAVIOR OF TiC-BASED CERMET

In the combustion synthesis, the ignition characteristics are determined through the use of different experimental parameters, and understanding the ignition behavior of TiC-based composites requires understanding all the data surrounding the experiences. Various ignition methods result in various combustion processes. The ignition temperature is found to be sensitive to the particle size, using the thermite reactions, sintering additives, mechanical activation, surrounding atmosphere for samples, Hadi Ghazanfari and Carl Blais [21] demonstrated the thermal explosion of Fe_3Al–TiC cermet from elemental pow-

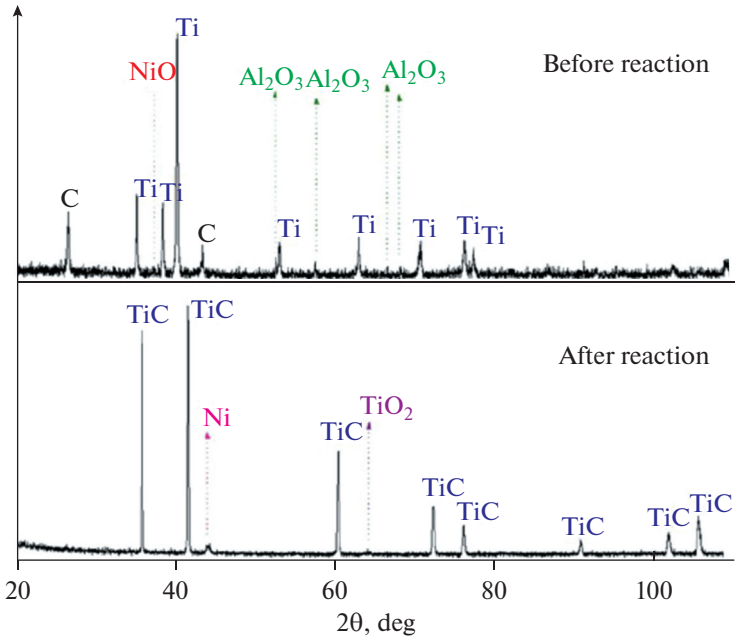

Fig. 2. XRD patterns of the sample 95%(Ti + C) +5%(3NiO + Al) + 10%Al_2O_3 [39].

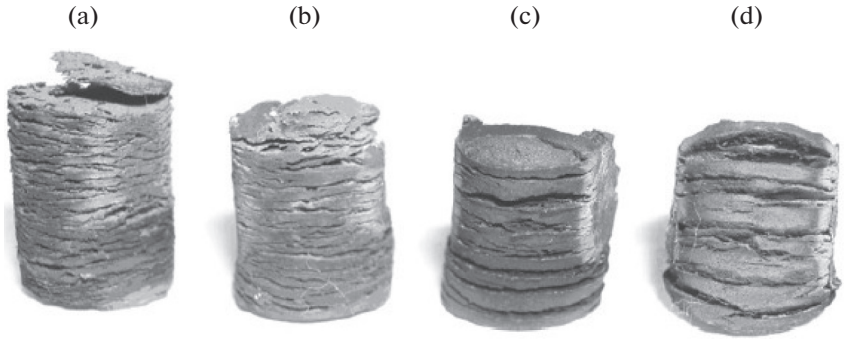

Fig. 3. TiC–Ni–Al_2O_3 cermets with different initial compositions [39]: (a) 80%(Ti + C) + 20%(3NiO + Al) + 5%Al_2O_3, (b) 75%(Ti + C) + 15%(3NiO + Al) + 5%Al_2O_3, (c) 90%(Ti + C) + 10%(3NiO + Al) + 5%Al_2O_3, and (d) 95%(Ti + C) + 5%(3NiO + Al) + 5%Al_2O_3.

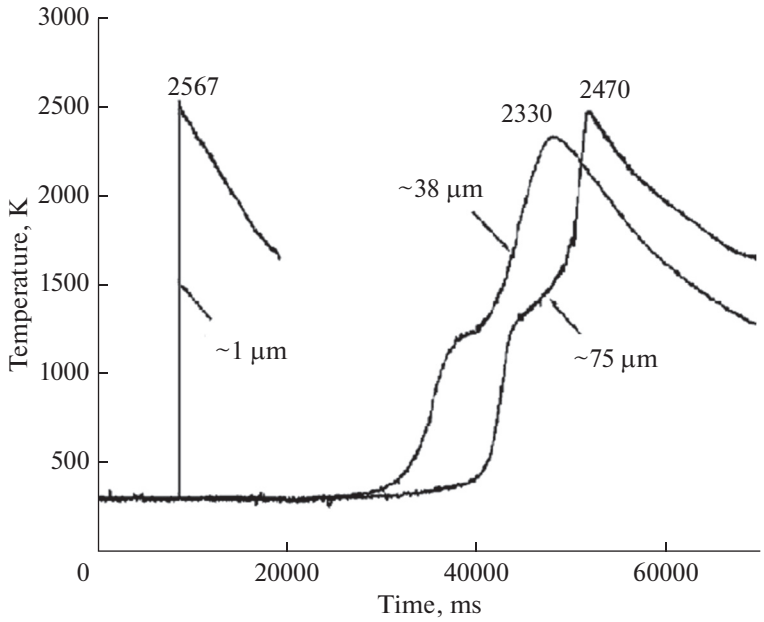

Fig. 4. Temperature–time profiles of 20 wt % Ni–Ti–C systems with C particle size of ~1, ~38, and ~75 μm during the SHS reaction [45].

ders in a furnace for 5 min with a heating rate of approximately 500°C/min. In this approach, premilling of reactants allowed not only the synthesis of the desired products (Fe_3Al–TiC) without intermediate phases but also reduced the furnace preheat temperature from 1200 to 1100°C. They demonstrated that TiC reaction is ignited at 1100°C [21]. Moreover, it was found that using fine particles is beneficial to avoid the formation of undesirable phases and leads to lowering the ignition temperature [21]. When the Ti particle size was about 100 μm, the (Ti + C) reaction started at around 1450°C, but this temperature decreased to 1206°C with using finer Ti particles (between 40 and 100 μm) [21, 44].

Likewise, the C particle sizes play an important role in the ignition behavior and combustion characteristics in the Ti–C–20 wt % Ni system as presented in Fig. 4. Coarse C particles (~38 and ~75 μm) led to the appearance of two different combustion stages, the first and second ones were related to the formation of Ni–Ti compounds and TiC ceramic, respectively. The SHS reactions were incomplete with a few Ni–Ti compounds and unreacted C. In contrast, using fine C particle (~1 μm), led to only one combustion stage and the final products consisted of TiC and Ni without any intermediate phase. Note that reducing C particle size caused an increase in the wave velocities and the ignition time became shorter. In addition to that, the morphology of TiC particles became almost spherical when decreasing the C particle sizes [45].

In another investigation, the ignition temperature of TiC–TiB_2/Ni cermet prepared by pressure assisted SHS from Ni–Ti–B_4C in air was 415°C that was lower

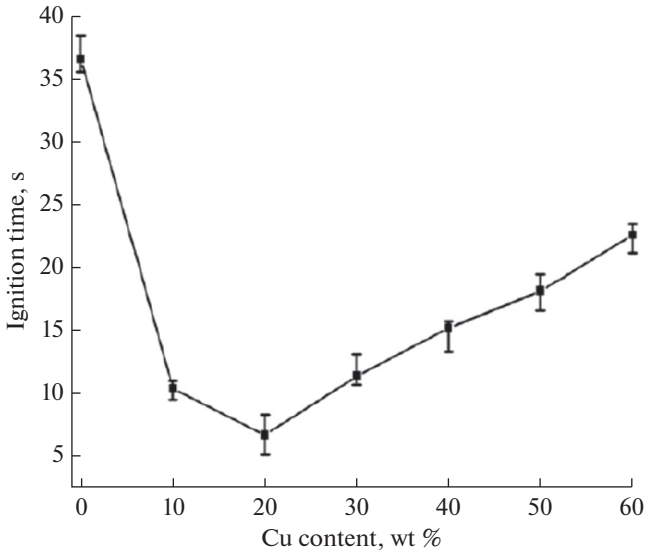

Fig. 5. The variation of the ignition time in the Cu–Ti–C systems with various Cu contents [47].

than that in vacuum (1040°C). This result was due to the heat generated from the oxidation and nitrification of Ti and the nitrification of B_4C on the surface of compact at low temperature. In this study, the ignition temperature both in air and vacuum decreased with decreasing Ni content and Ti and B_4C particle sizes. The authors added that low Ni content and fine B_4C particle size is beneficial to the completion of the reaction [46].

The addition of metallic phase (as a binder) in the Ti–C system was considered in [47]. Cu addition serves as diluent and binder and as consequence plays an important role in the ignition behavior of the SHS process. It was found that the combustion temperature decreases with increasing Cu content, the ignition time decreases first and increases later (Fig. 5), and the system exhibits the shortest ignition time with the addition of 20 wt % Cu. The increase in the Cu content decreased the dwell time at high temperatures, and therefore the size of the particles turned to be finer (Fig. 6). Moreover, an increase in the metallic liquid phase surrounding ceramic particles rose the diffusion, reduced the driving force for ceramic particle growth, and prevented the sintering among ceramic particles to form larger ones [47].

A typical example of the influence of mechanical activation on the ignition temperature can be found in the following study. References [48, 49] reported that in the combustion synthesis of TiC composite from thermite mixture ($3TiO_2$–4Al–3C), the ignition temperature decreases from 1079 to 698°C after 24-h ball-milling of initial reactants [48, 49]. In [36], it was observed too that the addition of Fe to ($3TiO_2$–4Al–3C) mixture decreases the ignition temperature of the reaction between Ti and C when using the thermite reaction to obtain TiC–Al_2O_3–Fe cermet by SHS process.

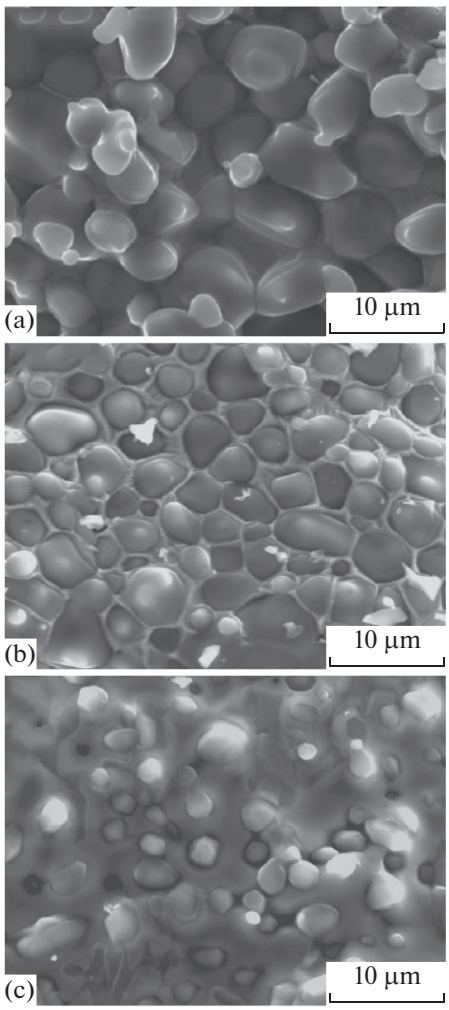

Fig. 6. The fracture surfaces of SHS products from Cu–Ti–C systems with (a) 10, (b) 30, and (c) 50 wt % Cu [47].

Reference [50] reported that the ignition temperature of NiAl–TiC–Al_2O_3 composites obtained using Ni/Al with 0, 10, 20, 30, and 40 wt % TiO_2/Al/C as additives is approximately 813.3, 852.6, 1005.3, 1039.6, and 1133.4 K, respectively. This means that the ignition can occur at a temperature below the melting point of Al (933 K), as the lowest melting point in the system. Authors explained this raise of the ignition temperature by that increasing the content of TiO_2/Al/C absorbs more heat released by the NiAl reaction as consequences the heat required to initiate the exothermic reaction of the system increases, it reduces the thermal conductivity of the sample due to the addition of low thermal conductivity material TiO_2, and results in a slower reaction rate of Ni/Al and it also reduces the contact between Ni and Al. Increasing the TiO_2/Al/C content led also to a longer ignition time. This was because a lower amount of TiO_2/Al/C had a higher content of the liquid NiAl in the product

Table 1. Adiabatic temperatures T_{ad} of TiC-based composites synthesized by SHS method.

No.	TiC-based composites	T_{ad} (K)	References
1	TiC	3210	[33, 54]
2	Fe_3Al–30 mol % TiC	2102	[21]
3	Fe_3Al–50 mol % TiC	2496	[21]
4	Fe_3Al–70 mol % TiC	2887	[21]
5	Ti–1.0 wt % C Ti–8.26 vol % TiC	1347	[21]
6	Ti–2.1 wt % C Ti–17.51 vol % TiC	1435	[21]
7	Ti–4.2 wt % C Ti–35.59 vol % TiC	1599	[51]
8	Ti–6.3 wt % C Ti–54.26 vol % TiC	1789	[51]
9	TiC	3300	[53]
10	TiC–5Ni	3144	[53]
11	TiC–10Ni	3144	[53]
12	TiC–15Ni	3144	[53]
13	TiC–20Ni	3037	[53]
14	TiC–10 wt % Al	2767	[55]
15	TiC–20 wt % Al	2767	[55]
16	TiC–50 wt % Al	1660	[55]
17	TiC	3290	[47]
18	TiC–10 wt % Cu	~2900	[47]
19	TiC–50 wt % Cu	~2400	[47]
20	TiC–TiB_2	~3200	[56]
21	TiC–TiB_2–10 wt % Co	~3200	[56]
22	TiC–TiB_2–50 wt % Co	~2300	[56]
23	Ti–0.75 C	2920	[57]
24	NiAl–TiC–Al_2O_3	2325	[50]
25	90(Ti + C) + 10Ni	3047	[28]

which, in turn, increased the thermal conductivity of the reactant [50].

4. ADIABATIC TEMPERATURE CHARACTERISTICS

The variations of the adiabatic temperatures of TiC-based materials synthesized by SHS are collected in Table 1. Literature cited that the experimental parameters such as stoichiometry [51, 52], particle size of raw materials [21, 44], increasing the TiC percentage [21] or additional component in the final cermets [53], mechanical activation before combustion synthesis [52] affect not only the heat release but also the kinetics of the reaction and the adiabatic temperature of the SHS process.

Results showed that the adiabatic temperature increases from 2102 K for Fe_3Al–30TiC to 2887 K for Fe_3Al–70TiC (Table 1, nos. 2–4) and the values are well greater than the melting point of Fe_3Al (1723 K) [21, 58], then, an increase in TiC contents in the final cermets leads to rising in the adiabatic temperature values of the combustion synthesis considering that the titanium carbide formation reaction is an exothermic reaction, however the addition of Fe–Al to the initial mixture acts as a diluent for this reaction [21].

Mechanically activated Ti–xC powder mixtures (x = 1.0, 2.1, 4.2, and 6.3 wt %) were synthesized in thermal explosion mode in a furnace preheated to 800°C by G.A. Pribytkov and A.V. Baranovskiy [51]. Combustion products were (metal matrix) Ti–TiC composites containing different quantities of reinforcement agent (Table 1, nos. 5–8). T_{ad} was found (Fig. 7) to grow linearly with increasing the mass percentage of C in the starting powder and reach its maximum at 1516°C, which is 164°C below the Ti melting point. This implies that combustion reaction occurred in a solid state reaction. Reference [51] also reported that the maximum combustion temperature T_{max} grows with increasing the mass proportion of C in the initial powder but always remains below T_{ad} by 490–530°C.

The researchers of [53] studied the effect of the addition of binder–polyvinyl butyral (PVB) on the adiabatic temperature and burning velocity of granulated (Ti + C) + xNi ($x \le 20$ wt %) mixtures. Figure 8 shows measured burning velocities U for mixtures 1 containing 2 wt % PVB and mixture 2 with 1 wt % PVB in comparison with burning velocity U_0 of granules containing no PVB (curves *1*, *2*, and *4*, respectively). One can see that, for both mixtures, the burning velocity decreases with increasing Ni content, which correlates with a reduction in adiabatic temperature (Table 1, nos. 9–13) [53].

In another work, S. Rogachev and S.G. Vadchenko [59] reported the SHS of TiC–high entropy alloy (HEA) CoCrFeNiMe (Me = Mn, Ti or Al). They found that both adiabatic temperature and burning velocity decrease with increasing mass fraction of CoCrFeNiMe binder (m_b) as represented in Fig. 9. Such dependencies were predictable because only the reaction (Ti + C) had strong exothermic effect, while the HEA binder did not produce significant heat release. When the adiabatic temperature decreased below the melting point of Ti, self-propagating synthesis became impossible. This limit occurred at m_b = 55 wt % for CoCrFeNiMn binder, 60 wt % for CoCrFeNiTi, and 45 wt % for CoCrFeNiAl. The combustion became unsteady, oscillating or spinning, near combustibility limits (dashed lines in Fig. 9) [59].

The WC–TiC–Al_2O_3 composite was the result of the self-propagating high-temperature synthesis of the double thermite reactions of WO_3–TiO_2–Al–C. The

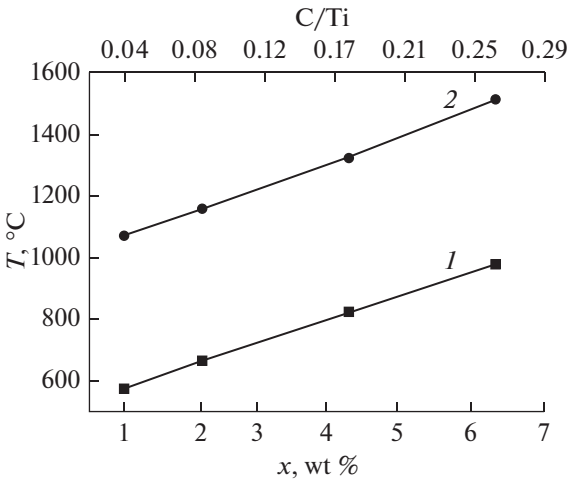

Fig. 7. Measured (*1*) and adiabatic (*2*) combustion temperatures as a function of *x* in the Ti–*x*C powder mixtures [51].

adiabatic temperature of the WO_3–Al–C system was 3995 K; this value is higher than those previously reported in Table 1. However, T_{ad} reached the minimum which corresponds to 2351 K for the TiO_2–Al–C system. Bowen and Derby [60, 61] showed that the combustion front velocity in the TiO_2–Al–C system decreases with the addition of the Al_2O_3 diluent because it reduces the adiabatic temperature [60, 61]. It was found in [61] that replacement of WO_3 with TiO_2 in the reactants decreases both the adiabatic temperature and combustion front velocity in a similar manner.

During SHS processing of the TiC–Al cermet according to the reaction Ti + C + *x*Al = TiC + *x*Al, Al additive played an important role in determining the size, morphology, and formation path of TiC particles**.** But with Al content increasing, the adiabatic temperature, combustion temperature and sizes of TiC particles decreased greatly (Table 1, nos. 14–16) [55]. The T_{ad} values as a function of Al content in the blends are shown in Fig. 10. As seen, T_{ad} rapidly decreases with Al content increasing except for a plateau with Al content ranging from 10–20 mass %, where T_{ad} stays at 2767 K corresponding to the boiling point of Al. The appearance of the plateau resulted from the absorption of heat from the evaporation of Al. Once Al content reaches 50 mass %, T_{ad} is just 1660 K, which is much lower than 1800 K. When Al content is up to 50 mass %, T_c is only 1630 K, leading to the failure of SHS reaction in Al–Ti–C system [55] but reaction can be ignited and self-sustaining combustion without external heat supply if $T_{ad} > 1800$ K [62].

It was found in [36] that adding Fe to the ($3TiO_2$ + 4Al + 3C) thermite mixtures from 0 to 15 wt % decreases the combustion front velocity and the SHS reaction auto quenches at 20 wt % Fe addition. Thus, the SHS reaction became unstable when the amount of added Fe increased from 15 to 20 wt %, (i.e.,1.21–1.71 mol). The adiabatic temperatures of samples containing 15 and 20 wt % Fe were 2157 and 1790 K, respectively. The last one appears lower than 1800 K (Fig. 11) [36].

The SHS method combined with direct consolidation for simultaneous synthesis and densification of

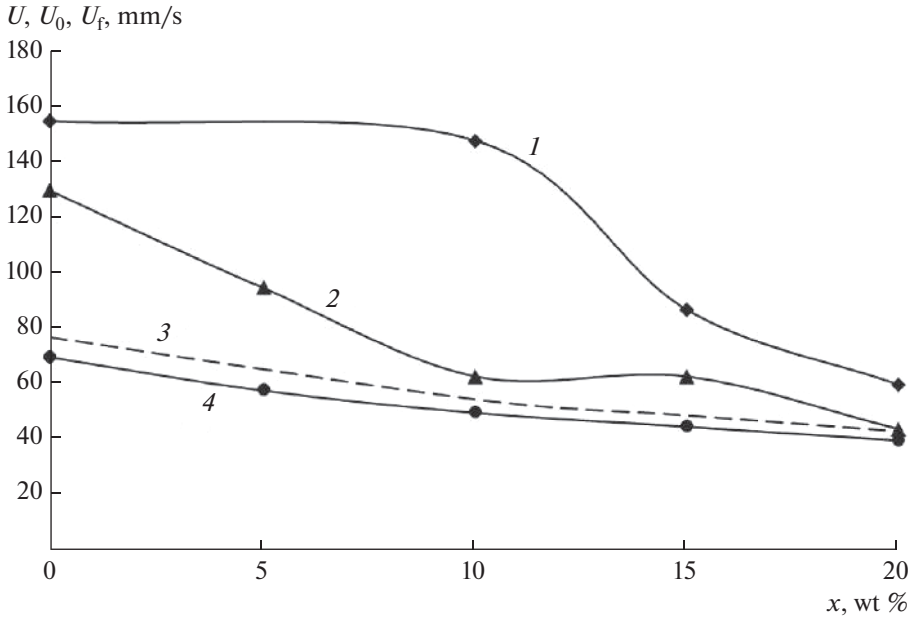

Fig. 8. Burning velocities as a function of *x* of granulated (Ti + C) + *x*Ni. *U* for blends 1 (solid curve *1*) and blends 2 (solid curve *2*); U_0 for granules containing no PVB (solid curve *4*); U_f calculated values for blends 1 (dashed line *3*) [53].

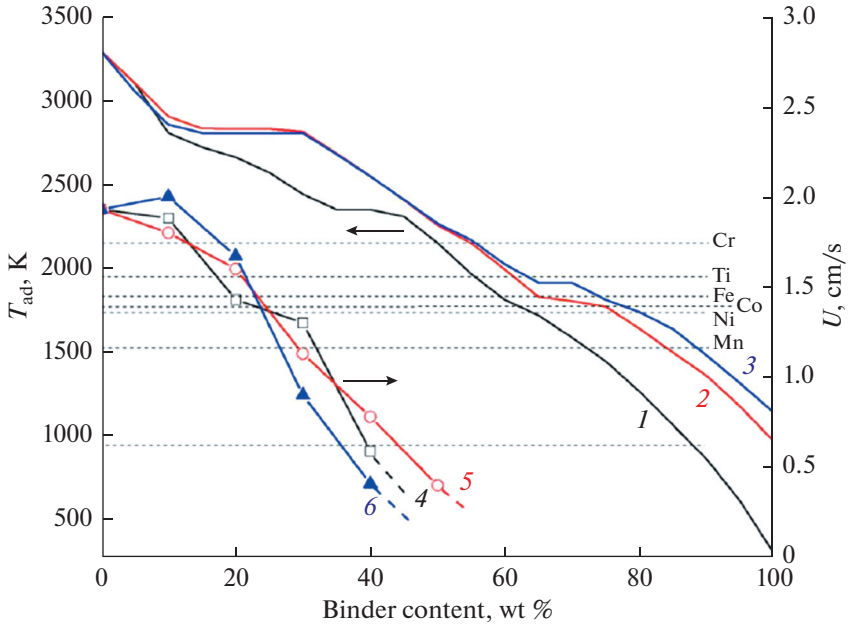

Fig. 9. The adiabatic temperatures (*1*–*3*) and burning velocities (*4*–*6*) for TiC–HEA systems with different HEA binders: (*1*, *4*) CoCrFeNiMn, (*2*, *5*) CoCrFeNiTi, and (*3*, *6*) CoCrFeNiAl. The horizontal dashed lines show the melting temperatures of starting reagents [59].

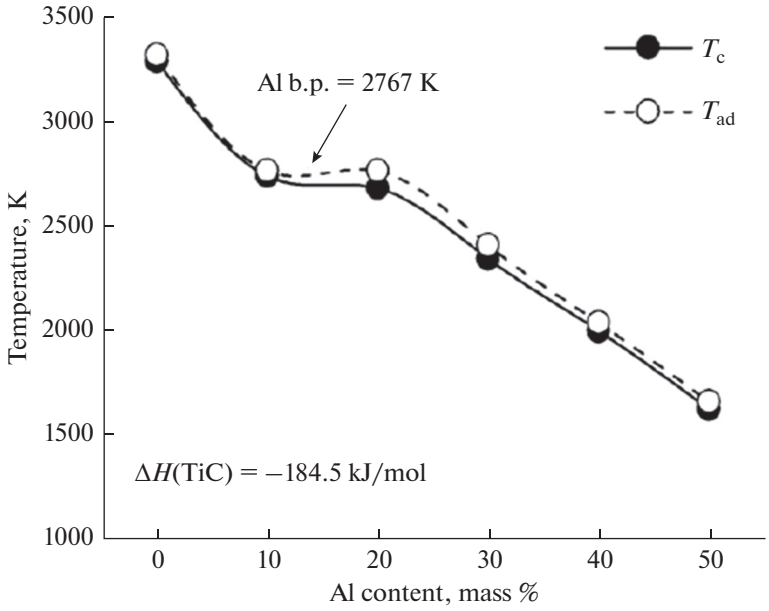

Fig. 10. Adiabatic temperature T_{ad} and combustion temperature T_c as a function of Al content [55].

TiC/Al_2O_3 composite from TiO_2, Al and C powders presented a linear relation between the calculated adiabatic temperature T_{ad} and different initial temperatures T_0 [63]. Results showed that the adiabatic temperature of the reaction at 298 K is 2403 K. This temperature increased linearly with increasing initial temperature T_0. These calculations indicated that the value of T_{ad} is higher than that of the empirical value (1800 K) which means that the reaction between TiO_2, Al and C proceeds in a self-sustaining mode. Also, this temperature exceeded that of the melting point of Al_2O_3 (2323 K) which indicates that the alumina phase was in the molten state during combustion. On the other hand, TiC phase was in the solid state because

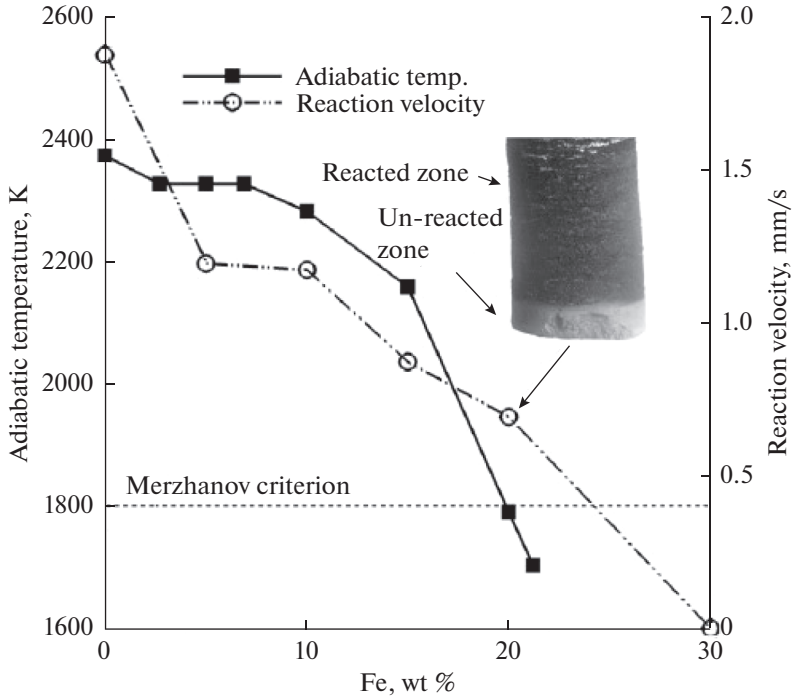

Fig. 11. Simultaneous effects of Fe addition on combustion velocity and adiabatic temperature of reaction ($3TiO_2 + 4Al + 3C + x$Fe) [36].

the adiabatic temperature is lower than the melting point of TiC (3100 K) in this study [63].

5. DIFFERENTIAL THERMAL ANALYSIS STUDY

M. Rezaeezadeh and M. Shafiee Afarani [61] reported the self-propagating high temperature synthesis of WC–TiC–Al_2O_3 composite powder. Their thermal analysis results confirmed that the aluminothermic reductions of WO_3 and TiO_2 are the first exothermic reactions initiated the SHS process. DSC curves of $2WO_3$–4Al–2C, $3TiO_2$–4Al–3C, and $0.8WO_3$–$1.8TiO_2$–4Al–2.6C systems are shown in Fig. 12. We can see several thermal events in these curves; endothermic peaks at around 657°C relating to the melting point of Al, exothermic ones are exposed in Fig. 12 and explained in Table 2 (nos. 1–3). There is a difference of interpretation about the nature of the exothermic event at 1170°C (Table 2, no. 2). References [61, 64] showed that this peak results from the reaction between Ti and C and consequently the formation of TiC, but others [36, 61, 65, 70, 71] showed that this peak is related to the formation of titanium aluminides in the form of intermediate phases, with no evidence of TiC formation. We add from references [36, 61] that no TiC was obtained while heating the $3TiO_2$–4Al–3C system up to 1250°C. To obtain TiC during SHS, it was indispensable for the formation of a molten phase rich in Ti or even in Ti_3Al. The melt accelerated the dissolution of carbon and facilitated the reaction between Ti and carbon, because the diffusion of solid carbon into Ti-rich solid phase needed long times which was beyond the SHS reaction time (a few seconds) [44, 61]. The DSC curve of $0.8WO_3$–$1.8TiO_2$–4Al–2.6C is presented in the curve (c). One can see a little overlapped events at 936 and 966°C which are caused by the aluminothermic reduction of WO_3 and TiO_2 in that order. In [61], the exothermic event at 1020°C was associated with the formation of WC, and the last one at 1221°C was due to the formation of titanium aluminide [57].

We note that the DSC results (Table 2) of systems are slightly varied, and this is mainly due to the raw mixtures used, as well as the operating conditions. Mixtures are heated at much slower heating rates in the DSC measurement than that in the SHS process that may make a significant difference in the determination of the reaction sequence and the formation of final products or intermediate phases, especially in the synthesis of complex phases by SHS. In another hand, the authors of references [21, 36, 44, 61, 64–66, 70, 71] agreed and stated that no reaction is observed before melting of Al when using aluminothermic reduction of oxides to produce TiC composite materials.

6. FORMATION MECHANISMS

6.1. Solid–Solid Reaction Mechanism

Heating rate has a significant influence on the mechanism and kinetics of the combustion synthesis

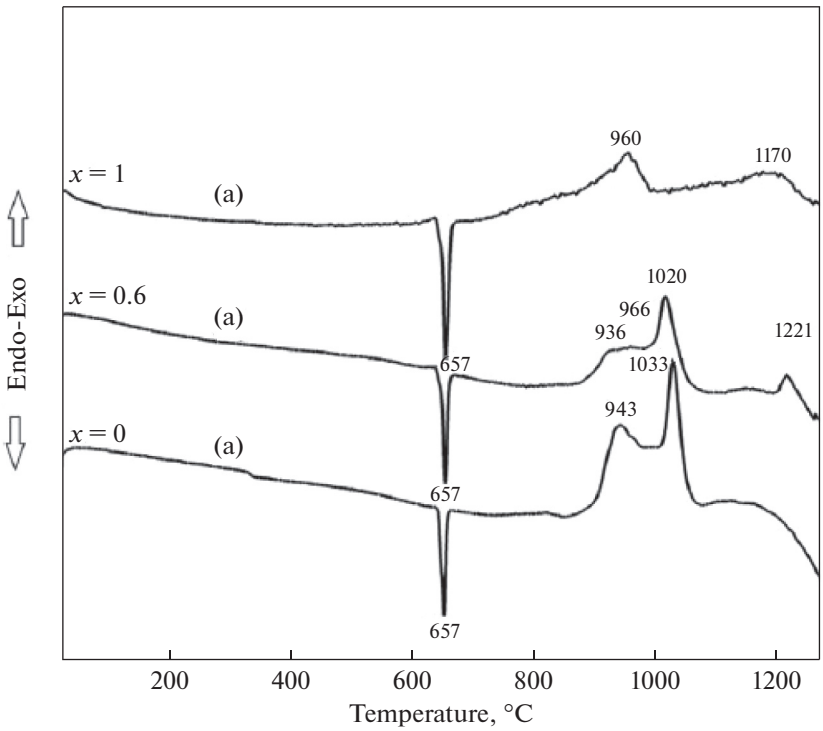

Fig. 12. DSC curves of (a) $2WO_3$–4Al–2C, (b) $3TiO_2$–4Al–3C, and (c) $0.8WO_3$–$1.8TiO_2$–4Al–2.6C systems [61].

method [21, 72–74]. In the SHS of (Ti + C) at heating rate lower than 250°C/min, it was found that the samples are not ignited even after reaching 1550°C [21, 44] This occurred due to the formation of TiC interfacial layer around Ti particles by solid-state reaction with carbon. But TiC phase formation was observed at 1165°C before the formation of the TiC interfacial layer at a higher heating rate (350°C/min), The close contact between carbon and Ti led to the formation of TiC either from solid-solid reaction or from reaction of carbon with Ti containing liquid solution according to equation (11) Ti + C= TiC [21, 75, 76].

6.2. Dissolution–Precipitation Mechanism

To understand this behavior, the researchers investigated the combustion of the Cu–Ti–C system. The SHS reaction starts with the solid diffusion reaction between the Cu and Ti particles, then the melting of Ti_xCu_y compounds occurs, the Cu–Ti liquid form and spread over the C particles. The C particles dissolve into the Cu–Ti liquid, resulting in the formation of the Cu–Ti–C ternary liquid; next, some TiC particles form firstly at the interface between the liquid and the C particles, where the carbon concentration is relatively high. With the increase in the temperature, carbon particles continue to diffuse into the Cu–Ti–C liquid and then TiC particles are gradually precipitated out from the liquid until the total consumption of carbon. So, the formation mechanism of TiC in the Me(metal)–Ti–C systems is always dissolution–precipitation (Fig. 13) [69].

In the same subject, another example is that of the combustion synthesis of the cermet TiC–high-entropy alloy (HEA). The reaction mechanism of the cermet TiC–HEA CoCrFeNiMe (Me = Mn, Ti or Al) involves three stages. First, all metallic components melt when the temperature in the combustion wave exceeds their melting points and form the Ti–Co–Cr–Fe–Ni–Me multi-component melt surrounded by solid carbon particles. After that, during the second stage, carbon dissolves in the melt and crystalline TiC grains precipitate and grow in the molten matrix. At the last stage, crystallization of the HEA binder occurs, when the sample temperature decreases below the melting point of this binder [59].

6.3. Mechanism Involving Thermite Reactions

6.3.1. System with one thermite reaction

During the SHS of NiAl–TiO_2–C systems, the composition of reactants was determined according to the following equations:

$$Ni + Al = NiAl, \quad (12)$$

$$3TiO_2 + 4Al + 3C = 2Al_2O_3 + 3TiC. \quad (13)$$

In this study, the product formation mechanism has three stages. The first one is initiated by the melting of Al and after the decomposition of the intermediate phase $NiAl_3$ at 854°C, the reaction mechanism is

Table 2. DSC results of number of blends used to produce TiC-based composites by the SHS method

No	Systems	Al melting point (°C)	Temperatures (°C) recorded and corresponding changes from DSC measurements	References
1	$2WO_3$–4Al–2C	657	943°C: Reduction of WO_3 with Al melts 1033°C: Reaction of C with W	[61]
2	$3TiO_2$–4Al–3C	657	960°C: Aluminothermic reduction of TiO_2 1170°C (conflict)	[61]
3	$0.8WO_3$–$1.8TiO_2$–4Al–2.6C	657	936°C: Aluminothermic reduction of WO_3 966°C Aluminothermic reduction of TiO_2 1020°C: Formation of WC 1221°C: Formation of titanium aluminide	[61]
4	$3TiO_2$–4Al–3C	669	925°C: Aluminothermic reduction of TiO_2 971°C: Formation of TiC phase	[64]
5	$3TiO_2$–4Al–3C	661	840°C: Aluminothermic reduction of TiO_2 930°C: Reaction between Ti and Al	[65]
6	$3TiO_2$–4Al–3C	666	1008°C: Reaction between Ti and Al to form Ti_3Al	[66]
7	Fe_3Al–50% TiC premilled for 30 min	–	No exothermic peak for the formation of TiC	[21]
8	Ti–C–20 wt % Ni	–	1180°C: Complete formation of TiC	[45]
9	Al–Ti–C with 30 wt % Al content	659	613°C: Al–Ti solid-state reaction to form $TiAl_3$ 757°C: solid-liquid reaction to form a large number of $TiAl_3$ after Ti dissolving into the molten Al 913°C: C will react with $TiAl_3$ metastable phase to form more thermodynamically stable TiC phase	[55]

Table 2. (Contd.)

No	Systems	Al melting point (°C)	Temperatures (°C) recorded and corresponding changes from DSC measurements	References
10	$(4 + x)Al + xCu + 3C + 3TiO_2$ milled for 30 h	–	782°C: Formation of Al_4C_3, Al_3Ti, and Al_2O_3 phases 940°C: Reaction between Al_4C_3 and Al_3Ti and consequently formation of TiC phase.	[67]
11	$(4 + x)Al + xCu + 3C + 3TiO_2$ 0-h mechanical alloying	660	871°C: Reduction of some TiO_2 by Al and formation of Al_3Ti intermetallic phase	[67]
12	$3NiO + 5Al + Ti + C$ 5-h activated powder mixture	660	825°C: NiO reduction and nickel aluminide formation ($3NiO + 5Al = 3NiAl + Al_2O_3$) 950°C: TiC formation	[68]
13	30 wt % Co–Ti–B_4C	–	1082°C: The appearance of Co–Ti melt and the formation of Ti, Co_xB ($x = 1, 2$), $CoTi_2$, Co_2C, and TiC 1210°C: Formation of TiB_2–TiC–Co cermet.	[56]
14	Al–Ti–C with 30 wt % Al	659	613°C: Al–Ti solid-state reaction to form some $TiAl_3$ compound 757°C: Solid-liquid reaction to form a large number of $TiAl_3$ after Ti dissolving into the molten Al 913°C: C will react with the $TiAl_3$ metastable phase to form the more thermodynamically stable TiC phase	[55]
15	30 wt % Ni–Ti–B_4C in air	–	564°C: Oxidation and nitrification of Ti 680°C: Oxidation of B_4C 1036°C: Liquid formation through the reversed eutectic reaction: $L \rightarrow Ni_2B$ and Ni_4B_3. 1180°C: Residual Ti and C atoms diffused into liquid to form Ni–Ti–B–C liquid and finally TiC and TiB_2 were precipitated	[46]
16	20 wt % Cu–Ti–C	–	887°C: Solid-state diffusion reaction between Cu and Ti particles to form Ti_xCu_y 966°C: Formation of Cu–Ti liquid phase through the eutectic reaction of Ti_2Cu and TiCu phases 1021°C: Formation of TiC–T_2Cu–C–Ti	[69]

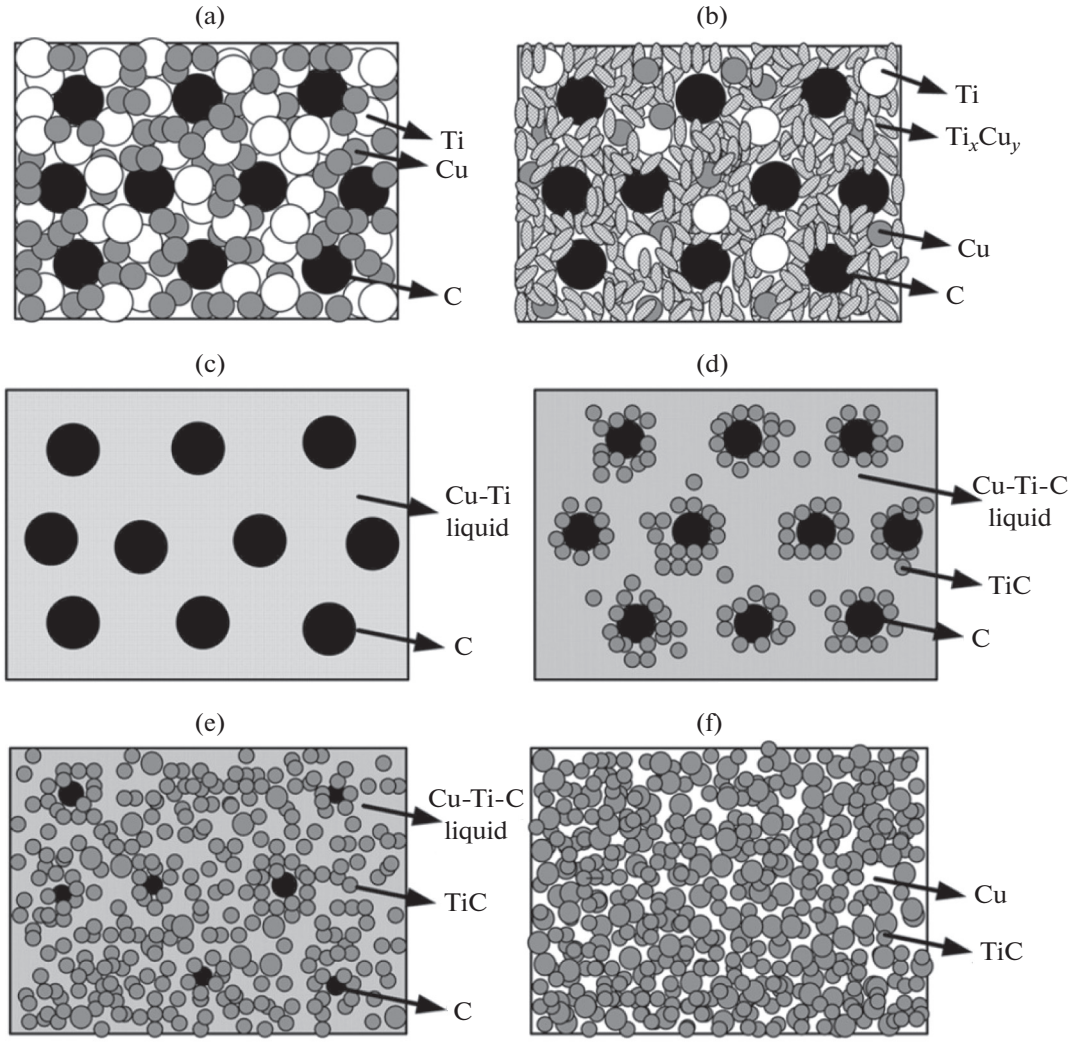

Fig. 13. The model corresponding to the mechanism of Cu–Ti–C system in the SHS process: (a) initial reactants, (b) formation of Ti_xCu_y compounds, (c) formation of Cu–Ti liquid, (d) and (e) TiC particles were gradually precipitated out of the liquid, and (f) fully reacted region [69].

the dissolution of solid Ni in the liquid Al. Other intermediate phases such as Ni_2Al_3 and Ni_5Al_3 can also be formed at this stage. In the second stage, the dissolution of Ni in the liquid Al occurs from 854°C to 1300°C. The third stage is dominated by the exothermic reaction of Ni + Al (heat of formation of reaction is ΔH_f (kJ/mol) = −118.4 [77, 78]). After the Ni + Al reaction is complete, the heat released by the formation of NiAl becomes the ignition agent to initiate further reactions in the TiO_2/Al/C system (ΔH_f (kJ/mol) = −1074.7 [69, 74–78]) to form TiC–Al_2O_3 phase. References [78–80] reported that the combustion process of TiO_2/Al/C systems involves two reactions: the metallothermic reduction of the oxide (TiO_2) to form an elemental Ti, and the reaction between Ti and C to form TiC. These reactions are described in equations:

$$4Al + 3TiO_2 = 2Al_2O_3 + 3Ti, \quad (14)$$

$$Ti + C = TiC \ (\Delta H_f\,(kJ/mol) = -184.5\ [46]). \quad (15)$$

6.3.2. System with double thermite reactions

The complexity of the mechanism of formation of ceramic–metal composites is illustrated by the result of the self-propagating high-temperature synthesis of the FeAl–TiC–Al_2O_3 cermet involving the double thermite reactions:

$$0.6Fe_2O_3 + 0.6TiO_2 + (y+2)Al + (y-1.2)Fe + 0.6C \rightarrow yFeAl + 0.6TiC + Al_2O_3. \quad (16)$$

The formation mechanism can be described by a series of steps as presented below. Aluminothermic reduction of Fe_2O_3 is considered as the initiation step as seen in reaction (17) $Fe_2O_3 + 2Al \rightarrow 2Fe + Al_2O_3$ followed by reduction of TiO_2 by Al in reaction (18)

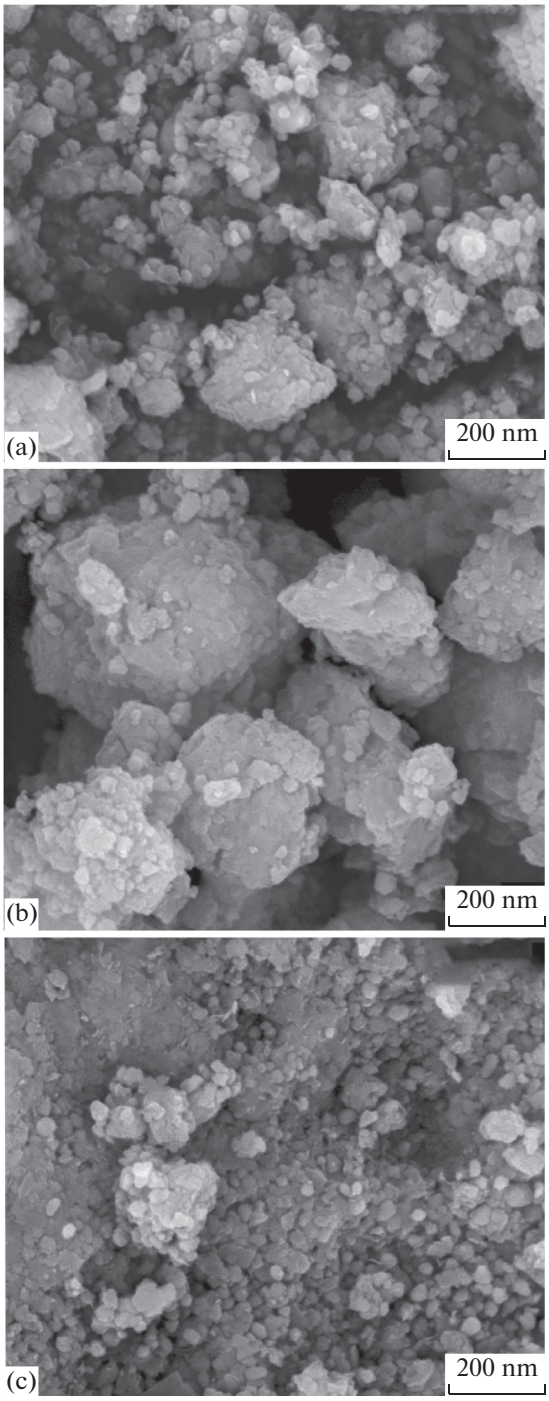

Fig. 14. SEM micrographs of Mg–TiC nanocomposite after (A) 60 h and (B) 70 h of mechanical alloying and (C) combusted powders (C) [82].

$TiO_2 + 4/3Al \rightarrow Ti + 2/3Al_2O_3$. Two reduction reactions do not only produce metal elements (Fe and Al), but also generate a substantial amount of heat to facilitate subsequent reactions. They include metal combustion between Fe and Al to form FeAl in reaction (19) Fe + Al → FeAl, as well as the reaction of Ti with carbon in reaction (15) to yield TiC [49].

7. RELATIONSHIPS BETWEEN STRUCTURE, MICROCTRUCTURE, AND MECHANICAL PROPERTIES

TiC is one of the promising reinforcements used in Mg matrix to augment and ameliorate its mechanical and physical properties [81, 82]. And in this regard, Mg–TiC@NiO nanocomposite powders were synthesized by combustion technique and the magnesiothermic reduction:

$$3Mg + TiO_2 + C = Mg + TiC + 2MgO. \quad (20)$$

This preparation is made through depositing a thin layer of NiO on the Mg–TiC composite. The starting powders were milled at 360 rpm for a maximum of 70 h. The hardness of Mg–TiC nanocomposite ball-milled for 60 h (Fig. 14a) shows a 42.37% increase as compared to that in pure magnesium and as stated in [81, 82], the presence of TiC particles inhibits dislocation motion and increases the hardness of the Mg matrix composite. An increase in the milling time to 70 h (Fig. 14b) decreased the hardness from 73.69 to 68.72 HV. However, the results showed that the maximum value of hardness (96.9 HV) was observed in the Mg–TiC@NiO combusted powders (Fig. 14c).

The compressive test (Fig. 15) showed that the deposition of a thin (approximately 3 to 4 nm) layer of NiO (Fig. 16) on Mg–TiC particles manages to improve the strength up to 625 MPa but for the Mg–TiC nanocomposite ball-milled for 70 h the value (499 MPa) was lower than that of specimen ball-milled for 60 h (532 MPa). This result can be attributed to the overall particle size of the TiC reinforcements, which is 20 and 49 nm for 60-h and 70-h milling, respectively (Figs. 14a and 14b). The increase in particle size is related to the agglomerates formed during contact between the molten magnesium and other particles during milling [82].

Changing the amount of the TiC compound in the final composites has a significant effect on their mechanical behavior. In this view, reference [50] reported that the higher content of the TiC and Al_2O_3 in the combusted product NiAl–TiC–Al_2O_3 cermet as the result of the addition of TiO_2/Al/C into Ni/Al mixtures improves their microhardness as revealed in Fig 17. Reference [49] reported that ceramic phases, TiB_2/Al_2O_3 and TiC/Al_2O_3, increase the hardness of FeAl composites from 12.8 to 16.6 GPa while maximum fracture toughness values of the TiB_2/Al_2O_3- and TiC/Al_2O_3-added FeAl composites are 9.84 and 9.16 MPa $m^{1/2}$, respectively. Hongwei Zhao and Jinhong Li [30] demonstrated that the content of TiC has an important influence on the hardness of the ZTA–TiC–FeCrNi cermet samples prepared by high-gravity combustion synthesis. With increasing content of TiC the hardness gradually increases as shown in Fig. 18 [43] and this is the result of two factors. The first is the intrinsic high hardness of TiC, and the second is microstructure refinement and thus enhanced interfa-

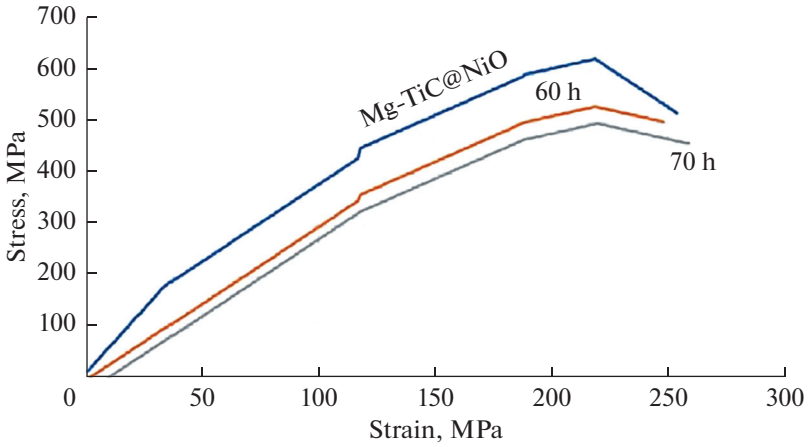

Fig. 15. Compressive stress–strain curves of 60- and 70-h milled Mg–TiC nanocomposite and Mg–TiC@NiO combusted specimens [82].

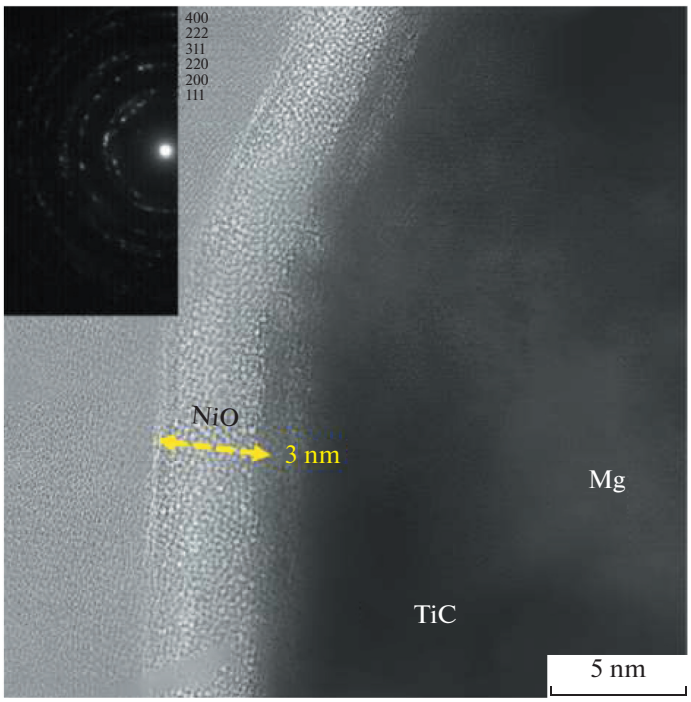

Fig. 16. TEM image of Mg–TiC@NiO [82].

cial area with increasing TiC content. In the range from 5 to 20% the hardness increases slowly with increasing TiC content and the volume fraction of TiC is lower than that of FeCrNi, and then the FeCrNi/TiC phase keeps ductile. However, the hardness increases quickly in the range from 20 to 30% because at a higher TiC content, the volume fraction of TiC exceeds that of FeCrNi, and the FeCrNi/TiC phase become brittle, thus resulting in a clearly improved hardness. In contrast to the hardness, the strength and toughness of the ZTA–TiC–FeCrNi cermets do not always increase with increasing content of TiC and the maximum strength and toughness are obtained with 20% TiC [30]. In the study of $CoCrFeNiAl_{0.2}(TiC)_x$ (x = 0, 0.06, 0.12, and 0.2) composites prepared by high-gravity combustion synthesis (HGCS) and as shown in Fig. 18a, the compressive strength of $CoCrFeNiAl_{0.2}(TiC)_x$ increases with the enlarged content of TiC from 1083 MPa at $x = 0$ to 2133 MPa at $x = 0.2$, but the fracture elongation decreases. The Vickers hardness tends to increase from 263 HV at $x = 0$ to 1183 HV at $x = 0.2$, and the bending strength of the composites firstly increases then decreases with increasing TiC content (Fig. 18b).

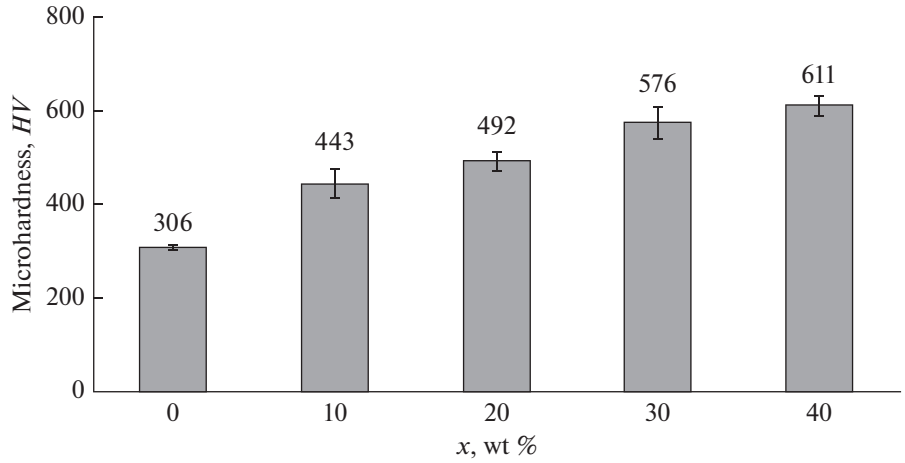

Fig. 17. Microhardness of synthesized products prepared from $(1 - x)$Ni/Al + x(TiO_2/Al/C) with x = 0, 10, 20, 30, and 40 wt % [50].

However, the raise in TiC content is not always positive and favorable. It is seen that when this value increases, many cleavage fracture surfaces appears and the fracture mechanism of the $CoCrFeNiAl_{0.2}(TiC)_{0.2}$ changes to the brittle fracture.

The size and distribution of the synthesized TiC were sensitive to the change of the value of the high-gravity field σ (Figs. 19b and 19c) and it was found that the rate of micro-pores in the composites decreases significantly with the increase in σ which can significantly improve the mechanical strength of the material. In another result, when increasing the content of Ti, C and enlarging the value of the high-gravity field, the TiC precipitate sizes increase from submicron to micron, which means that the grain refinement of the alloy matrix decreases, resulting in the decrease of the mechanical properties of composites. Figure 19a presents the relationship between the value of σ and the formation of BCC phase in final samples. It was found that the synthesized TiC and the small amount of BCC phase are accompanied by enhancing the compressive strength, bending strength, and hardness of composites by refining the grain of HEA [43].

It can be seen from Fig. 20 that the workhardening rate of the composite 50 vol % (TiC + TiB_2)/Al with Mg addition prepared by combustion synthesis and hot-pressing method is the highest, and this can improve the workhardening ability of the cermet, which makes it more capable of accumulating dislocations and hindering deformation. The solution strengthening resulted in severe dislocation multiplication and improved work hardening capacity, at the same time it reduced the rate of movable dislocations and the ability of the soft phase α-Al to coordinate the composite deformation, and consequently, reducing the plasticity and toughness. The dislocation multiplication caused by work hardening leads to an important reduction in plasticity and ultimately decreases in the toughness of the composites [83].

Results revealed that the fracture mechanism of the composites 50 vol% (TiC + TiB_2)/Al composites with different alloy elements (Mg, Zn) is mainly the interface cracking between ceramic particles and Al matrix (Fig. 21). So, the interface plays an important role in the initiation and propagation of cracks. The ceramic particles were refined and increased as a result of the addition of Mg, and the stress concentration at the tip of crack was minimized by a big number of small ceramic particles evenly dispersed to prevent the crack initiation. In addition, ceramic particles can change the direction of the propagation path of the main crack and during the propagation process, micro cracks are formed. So, the crack elongates along the path of interface propagation and consumes more fracture energy, which ameliorates the toughness of the composite. Adding alloy elements reduce the fracture strain of the composite and consequently decrease the toughness, and the reason of this is the lattice distortion caused by solid solution strengthening and the stress concentration caused by dislocation accumulation [83].

The addition of 5 vol % Ta, Nb, and Zr to 70 vol % TiC/Al cermets prepared by combustion synthesis and hot-pressing method, respectively, refines the size of TiC ceramic particles. This can significantly reduce the rate and size of cracks and pores in the cermet microstructure too. Reference [29] reported that the main strengthening mechanisms of adding alloying elements to improve the mechanical properties of these cermets are solid solution strengthening, TiC grain refinement, and crystal mismatch at the Al/TiC interface. The decrease in mechanical properties at room temperature is mainly due to the generation of intermediate phases. Ta, Nb, and Zr elements generate (Ti,X)C (X = Ta, Nb, and Zr) solid solutions and

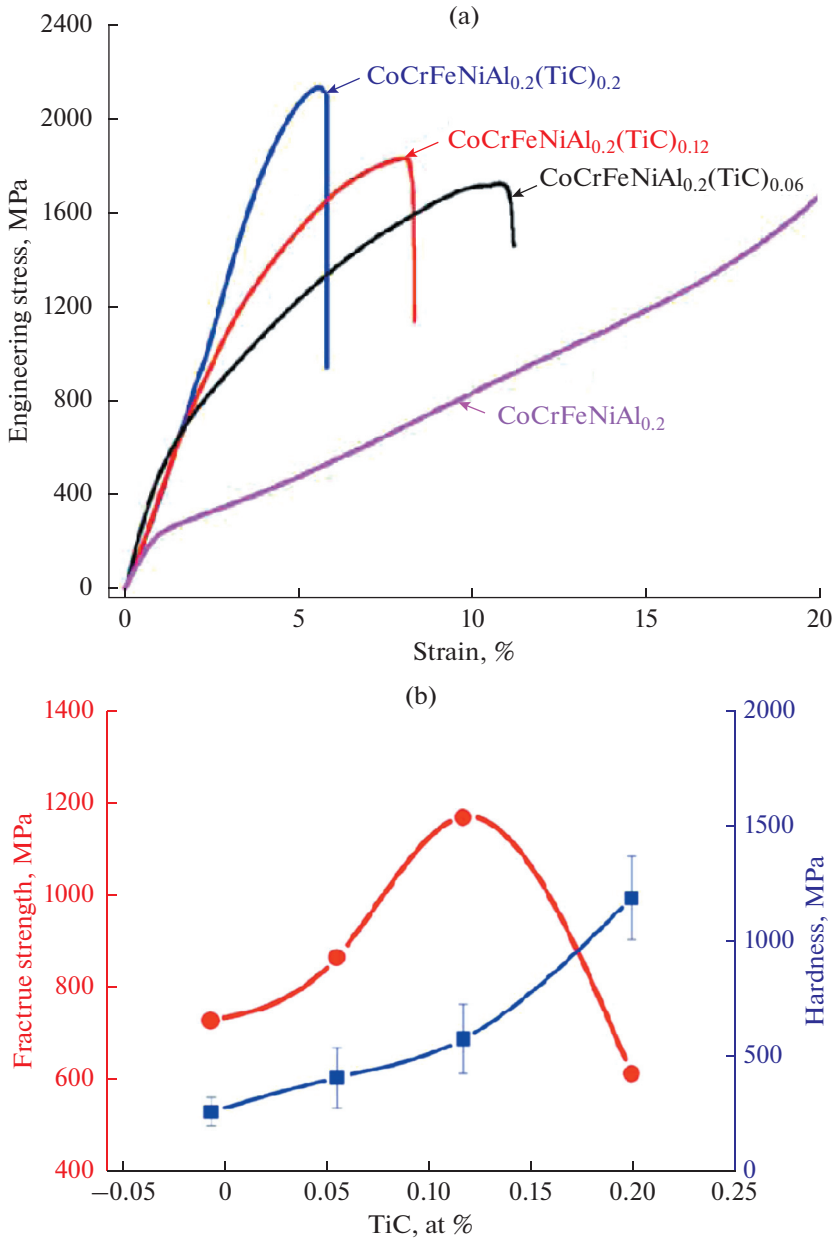

Fig. 18. Mechanical properties of $CoCrFeNiAl_{0.2}(TiC)_x$ (x = 0, 0.06, 0.12, 0.2) by HGCS with σ = 1200 g: (a) compressive stress–strain curves; (b) bending strength and hardness [43].

Al_3X (X = Ta, Nb, and Zr) intermediate phases during the reaction process, changing the lattice parameters of Al and TiC. As shown in Fig. 22, both (111) TiC and (111) Al diffraction lines shift to a lower degree as compared to cermet TiC/Al. It indicates that the solution of alloying elements into the aluminum matrix and TiC lattice may cause the lattice distortion of Al and TiC. TiC lattice expands, and its lattice constant becomes larger. The addition of Ta and Nb reduces the crystal mismatch at the Al/TiC interface [29].

Figure 23 shows the room temperature and high temperature (300°C) compression engineering stress–strain curves of TiC/Al, TiC/Al–Ta, TiC/Al–Nb, and TiC/Al–Zr. The yield strength ($\sigma_{0.2}$), ultimate compression strength (σ_{UCS}), and fracture strain (ε_f) of TiC/Al cermet at room temperature are 880.6 MPa, 978 MPa, and 8.47%, respectively, but results show that adding Ta and Zr at room temperature can increase $\sigma_{0.2}$ and σ_{UCS} and damage the ε_f value. In contrast, the addition of Nb reduces the $\sigma_{0.2}$, σ_{UCS} and ε_f of the combusted cermet. As for high-temperature (300°C) compression properties, the addition of Ta and Zr elements significantly increases $\sigma_{0.2}$, σ_{UCS} and ε_f. By comparison, the addition of Nb element can

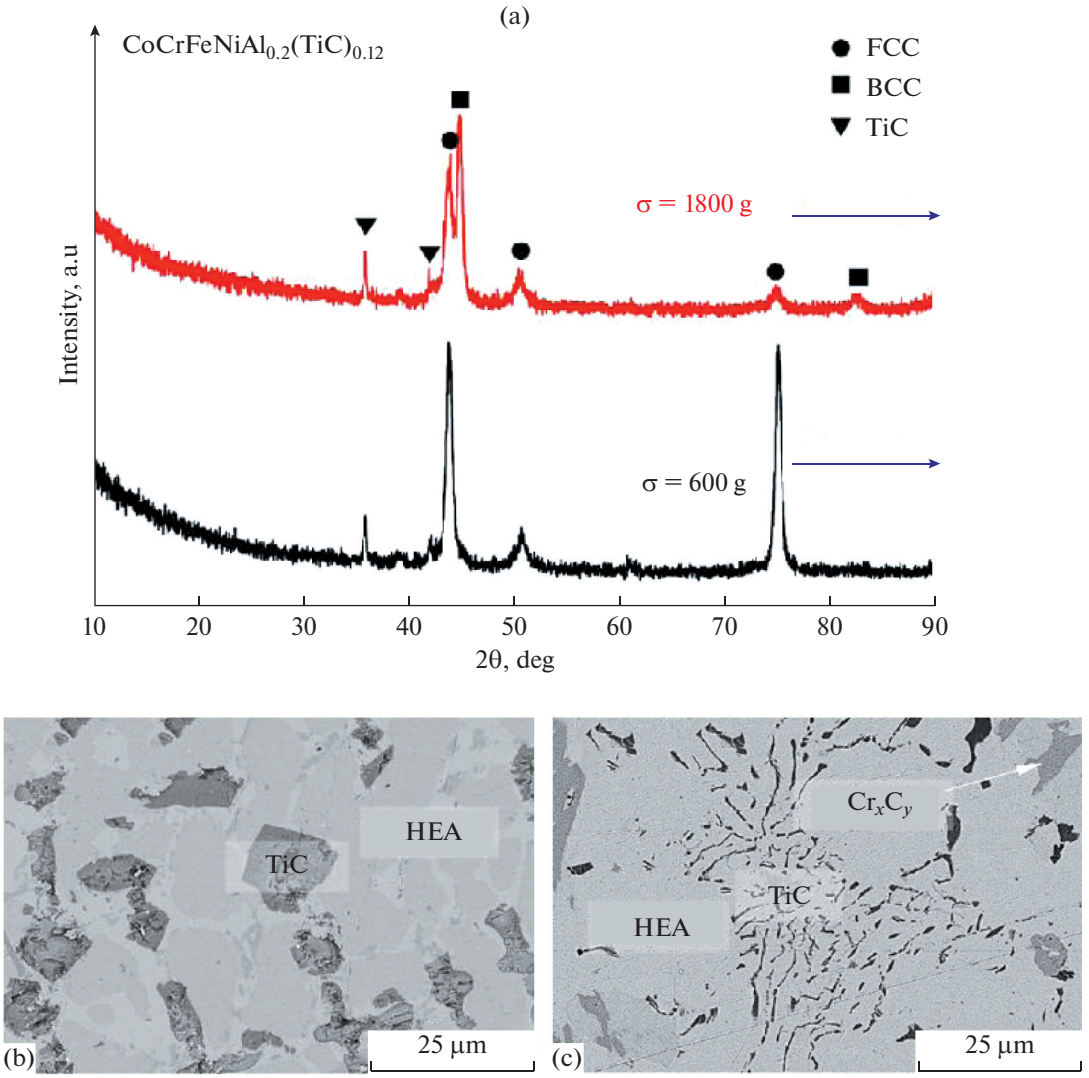

Fig. 19. (a) XRD patterns and SEM images of $CoCrFeNiAl_{0.2}(TiC)_{0.12}$ prepared by HGCS with different high-gravity field σ: (b) σ = 1800 g, (c) σ = 600 g [43].

improve σ_{UCS} and ε_f of the cermet, although slightly decreasing $\sigma_{0.2}$ [29].

According to [26, 84, 85], the strengthening and toughening of the ceramic are dependent on the defect size controlled by the refined microstructure, and also determined by fracture behavior of the ceramic able to present intensive toughening mechanisms. Due to the highest elastic modulus of TiB_2 as compared to TiC and Al_2O_3 (the average modulus of elasticity of TiB_2, TiC, and Al_2O_3 are 570, 450, and 400 GPa, respectively [26, 85]), TiB_2 phase releases the highest elastic strain energy among all phases in the solidified TiC–TiB_2 composite ceramics with a series of TiB_2 mole content, prepared by combustion synthesis in high-energy field, during fracture. That intercrystalline fracture usually takes place at the boundaries of TiB_2 platelets, except that transgranular fracture sometimes happens in some coarsened TiB_2 platelets containing defects and microcracks. Fine TiB_2 platelets play a predominant role in strengthening and toughening ceramic by initiating an intensive coupled toughening mechanism of crack deflection, crack-bridging and pull-out. The highest flexural strength of the TiC–50% TiB_2 (860 ± 35 MPa) benefits from the presence of the lowest content of Al_2O_3 inclusions, low content of minor Cr–W–Ti borides, and high-volume fraction of TiB_2. The achievements of fine-grained even ultra-fine-grained microstructure in the nearfull-density ceramic (98.7%) and high fracture toughness (13.5 ± 1.5 MPa $m^{0.5}$ for TiC–66.7% TiB_2 composite) contributed from an intensive coupled mechanism by a large number of fine TiB_2 platelets (Fig. 24) [85]. In

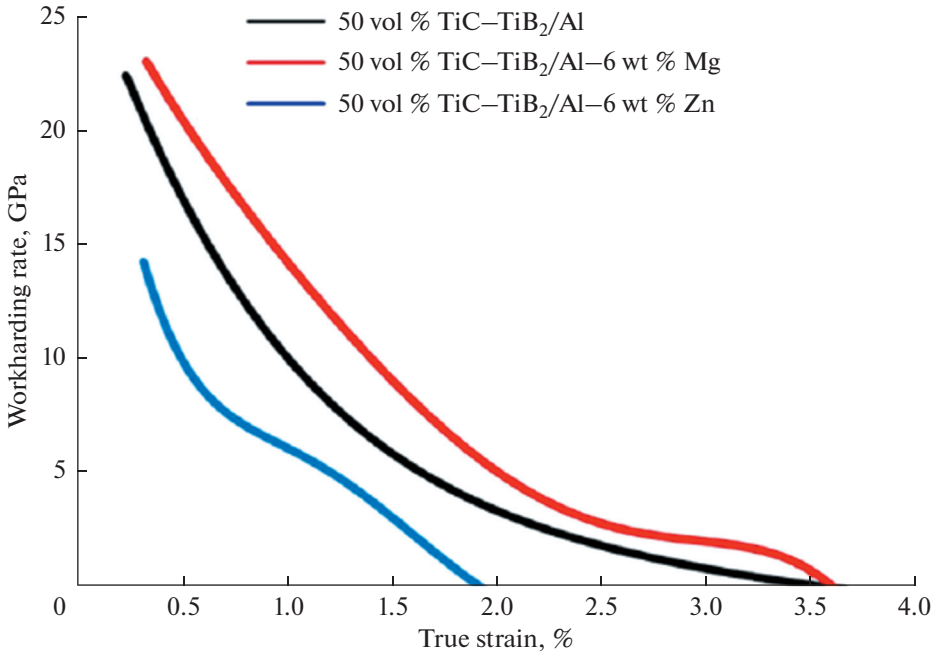

Fig. 20. Workhardening rate curves [83].

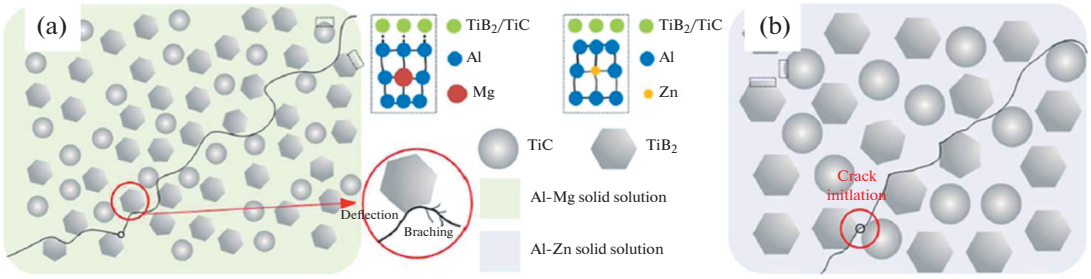

Fig. 21. Schematic of strengthening and fracture mechanism for (a) 50 vol % (TiC + TiB_2)/Al–6 wt % Mg and (b) 50 vol % (TiC + TiB2)/Al–6 wt % Zn [83].

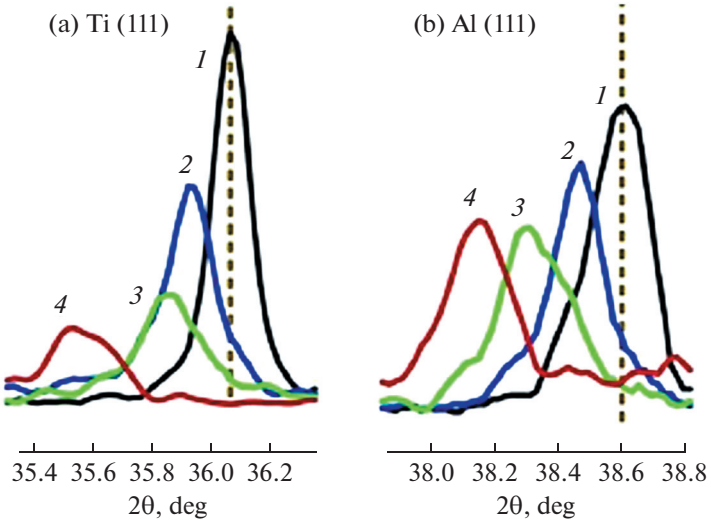

Fig. 22. The XRD patterns of (*1*) TiC/Al, (*2*) TiC/Al–Ta, (*3*) TiC/Al–Nb, and (*4*) TiC/Al–Zr samples: (a) diffraction peak of TiC (111); (b) diffraction peak of Al (111) [29].

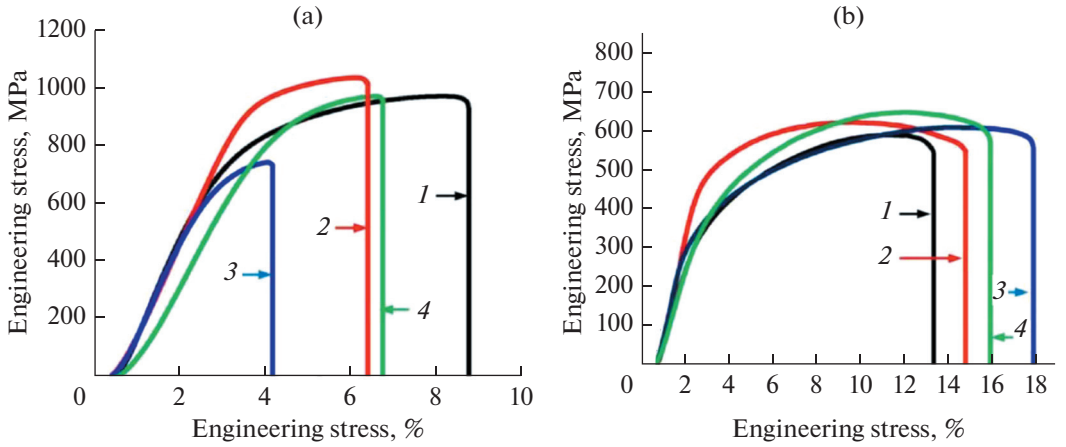

Fig. 23. Compressive engineering stress–strain curves of (*1*) TiC/Al, (*2*) TiC/Al–Ta, (*3*) TiC/Al–Nb, and (*4*) TiC/Al–Zr samples: (a) room temperature, (b) high temperature (300°C) [29].

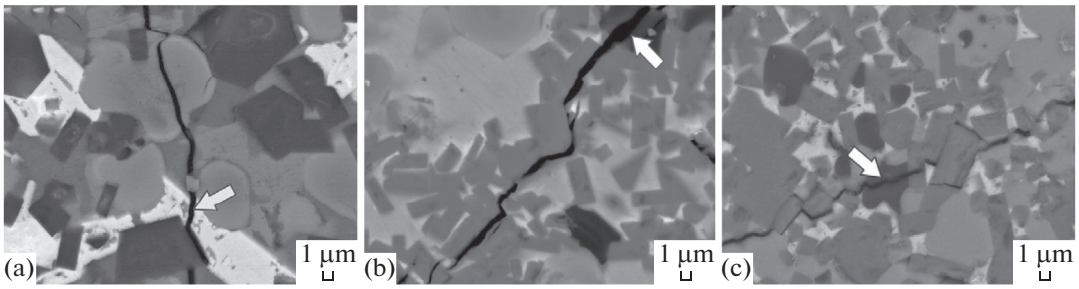

Fig. 24. Crack propagation paths of TiC–TiB_2 composite ceramics: (a) TiC–30% TiB_2; (b) TiC–40% TiB_2; and (c) TiC–66.7% TiB_2 [85].

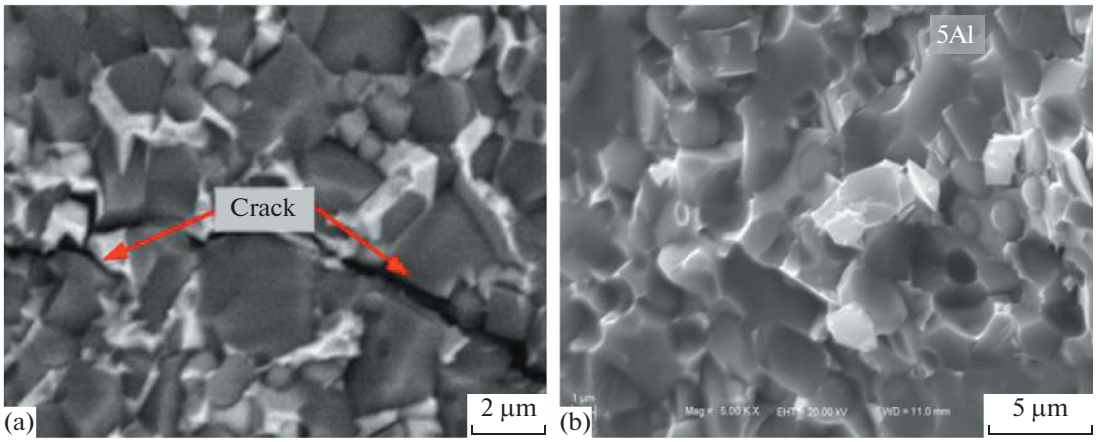

Fig. 25. Fracture surfaces of the (TiC_xN_y–TiB_2)/Ni composites with (a) 0 and (b) 5 wt % Al [86].

similar study, Figure 25 presents the fracture surfaces of the (TiC_xN_y–TiB_2)/Ni composites with 0 and 5 wt % Al prepared by combustion synthesis and hot press. Without the addition of Al, most of the cracks propagate along the ceramics–matrix interface, while with the addition of 5 wt % Al, most of the cracks propagate in the matrix and traverse some of the ceramic particles. This means that the addition of Al can improves the matrix strength between the ceramic particles and the matrix. The enhancement of the strength of final products when enlarging the Al addition is the result of the refinement of the ceramic microstructures, the

solid solution of Al in the Ni matrix, as well as the improvement of the interfacial bonding strength between the ceramics and the Ni matrix [86].

CONCLUSIONS

TiC-based composites can be successfully synthesized by self-propagating high-temperature synthesis (SHS) because of its numerous advantages such as dynamic of the combustion wave and high reaction rate that make reaction sequence possible, especially for the synthesis of complex phases like reactions including thermite ones.

Pre-milling of reactants increases the reaction kinetics, allows the synthesis of the desired products without intermediate phases, and reduces preheating and ignition temperatures of initial reactants.

Due to the large difference between the heating rate for DSC measurement and that required for combustion synthesis, determining the sequence of reactions varies according to the method adopted, particularly for complicated systems. Using low heating rates leads sometimes to the appearance of intermediate phases.

SHS exothermic reactions such as (Ti + C) involving thermite reactions are associated with high energy liberated and high adiabatic temperatures, consequently, the formation of the products occurs in the liquid phases.

Thermites are used to produce some additional energy to assist a particular synthesis reaction and Al_2O_3 can be employed as a diluent witch slows down the exothermic reactions.

The addition of metallic elements Cu and Al as a binder in the SHS of TiC to form cermets, serves as diluents and consequently, it affected the ignition behavior and adiabatic temperature, determining the size, morphology and formation of TiC particles.

Literature cited that the value of the adiabatic combustion temperature of TiC is in the region of 3210–3300 K. This value can be reduced when added metallic elements: Cu, Ni, Fe, Al.

The formation mechanism in the Metal–Ti–C systems is always dissolution–precipitation.

The formation mechanism of SHS process involving thermite reaction of TiC-based cermets can be described by a series of steps, and aluminothermic reduction of oxides is considered firstly. This reaction produces metal elements and generates a considerable amount of energy to assist subsequent reactions as well as the (Ti + C) reaction to form TiC.

TiC is one of the promising reinforcements used in metal matrix in the combustion synthesis of TiC-based composites in order to ameliorate their mechanical properties. The main strengthening mechanisms of adding alloying elements to improve these ones are solid solution strengthening and TiC grain refinement.

The strengthening and toughening of the final composite are also determined by its fracture behavior able to present intensive toughening mechanisms.

FUNDING

This work was supported by ongoing institutional funding. No additional grants to carry out or direct this particular research were obtained.

CONFLICT OF INTEREST

The author of this work declares that he has no conflicts of interest.

REFERENCES

1. Lu, H., Wu, L., Wei, H., Cai, J., Luo, K., Xu, X., and Lu, J., Microstructural evolution and tensile property enhancement of remanufactured Ti_6Al_4V using hybrid manufacturing of laser directed energy deposition with laser shock peening, *Addit. Manuf.*,2022, vol. 55, p. 102877. https://doi.org/10.1016/j.addma.2022.102877
2. Jiao, T., Jiang, T., Dai, G., Guo, Y., Sun, Z., Chang, H., Han, Y., Li, S., and Alexandrov, I.V., The microstructure evolution of TC_4–(TiB + TiC)/TC_4 laminated composites by laser melting deposition, *Mater. Charact.*, 2023, vol. 197, p. 112665. https://doi.org/10.1016/j.matchar.2023.112665
3. Fattahi, M., Delbari, S.A., Babapoor, A., Namini, A.S., Mohammadi, M., and Asl, M.S., Triplet carbide composites of TiC, WC, and SiC, *Ceram. Int.*, 2020, vol. 46, no. 7, pp. 9070–9078. https://doi.org/10.1016/j.ceramint.2019.12.155
4. Lou, Z., Li, Y., Zou, Q., Luo, W., Gu, H., Li, Z., and Luo, Y., Fabrication of the TiC matrix composite with the intragranular Al_2O_3 using carbon fibers as carbon source, *Mater. Charact.*, 2023, vol. 199, p. 112817. https://doi.org/10.1016/j.matchar.2023.112817
5. Sharma, A. and Karunakar, D.B., Influence of TiC addition on ablation and thermal shock behaviour of microwave sintered ZrB_2–SiC–TiC composites, *Ceram. Int.*, 2022, vol. 48, no. 23, pp. 34504–34515. https://doi.org/10.1016/j.ceramint.2022.08.031
6. Fattahi, M., Mohammadzadeh, A., Pazhouhanfar, Y., Shaddel, S., Asl, M.S., and Namini, A.S., Influence of SPS temperature on the properties of TiC–SiC composites, *Ceram. Int.*, 2020, vol. 46, no. 8, pp. 11735–11742. https://doi.org/10.1016/j.ceramint.2020.01.206
7. Szyma'nski, Ł., Olejnik, E., Sobczak, J.J., Szala, M., Kurtyka, P., Tokarski, T., and Janas, A., Dry sliding, slurry abrasion and cavitation erosion of composite layers reinforced by TiC fabricated in situ in cast steel and gray cast iron, *J. Mater. Process. Technol.*, 2020, vol. 38, p. 117688. https://doi.org/10.1016/j.jmatprotec.2022.117688
8. Xu, Z.-B., Kou, S.-Q., Yang, H.-Y., Dong, B.-X., Han, Y., Chen, L.-Y., Qiu, F., and Jiang, Q.-C., The effect of carbon source and molar ratio in Fe–Ti–C system on the microstructure and mechanical properties of in situ TiC/Fe composites, *Ceram. Int.*, 2022, vol. 48,

pp. 30418–30429.
https://doi.org/10.1016/j.ceramint.2022.06.319

9. Rahaei, M.B., Rad, R.Y., Kazemzadeh, A., and Ebadzadeh, T., Mechanochemical synthesis of nano TiC powder by mechanical milling of titanium and graphite powders, *Powder Technol.*, 2012, vol. 217, pp. 369–376.
https://doi.org/10.1016/j.powtec.2011.10.050
10. Lang, S., Yan, Q., Sun, N., Zhang, X., and Ge, C., Effects of TiC content on microstructure, mechanical properties, and thermal conductivity of W–TiC alloys fabricated by a wet-chemical method, *Fusion Eng. Des.*, 2017, vol. 121, pp. 366–372.
https://doi.org/10.1016/j.fusengdes.2017.07.026
11. Li, X., Liu, H., Hu, P., Wang, J., Yang, Y., and Li, H., Nanostructured TiC dispersion-strengthened tungsten composite with remarkably improved He ion irradiation resistance, *Int. J. Refract. Met. Hard Mater.*, 2022, vol. 107, p. 105900.
https://doi.org/10.1016/j.ijrmhm.2022.105900
12. Akhtar, F. and Guo, S., Microstructure, mechanical and fretting wear properties of TiC stainless iron composites, *Mater. Charact.*, 2008, vol. 59, pp. 84–90.
https://doi.org/10.1016/j.matchar.2006.10.021
13. Wang, Z., Zhou, M., Zhu, M., Jiang, Y., and Sui, Y., Effect of precursor density on the wear resistance of in-situ TiC/Fe matrix composites based on Fe–Cr system moderator, *Ceram. Int.*, 2023, vol. 49, pp. 18925–18936.
https://doi.org/10.1016/j.ceramint.2023.03.016
14. Wu, P.F., Shi, B.Y., Tu, H.B., Guo, C.Q., Liu, A.H., Yan, G., and Yu, Z.J., Pomegranate-type Si/C anode with SiC taped, well-dispersed tiny Si particles for lithium–ion batteries, *J. Adv. Ceram.*, 2021, vol. 10, pp. 1129–1139.
https://doi.org/10.1007/s40145-021-0498-6
15. Huanga, W., Zhao, S., Wang, J., and Xian, X., Fabrication of Si/TiC–SiC/C composites as high-performance anode materials for Li–ion batteries, *J. Phys. Chem. Solids*, 2022, vol. 171, p. 111019.
https://doi.org/10.1016/j.jpcs.2022.111019
16. Sharma, A. and Karunakar, D.B., Effect of SiC and TiC addition on microstructural and mechanical characteristics of microwave sintered ZrB_2 based hybrid composites, *Ceram. Int.*, 2021, vol. 47, pp. 26455–26464.
https://doi.org/10.1016/j.ceramint.2021.06.058
17. Wang, X.C., Zhao, J., Gan, Y.L., Tang, X.K., Gai, S.L., and Sun, X.S., Cutting performance and wear mechanisms of the graphene-reinforced Al_2O_3–WC–TiC composite ceramic tool in turning hardened 40Cr steel, *Ceram. Int.*, 2022, vol. 48, no. 10, pp. 13695–13705.
https://doi.org/10.1016/j.ceramint.2022.01.251
18. Guria, J.F., Bansal, A., Kumar, V., and Kumarc, B.V.M., Effect of co-addition of SiC and WC on the densification behaviour and microstructural evolution of TiC-based composites, *Ceram. Int.*, 2022, vol. 48, no. 9, pp. 12657–12691.
https://doi.org/10.1016/j.ceramint.2022.01.137
19. Li, L.Q., Fan, J.L., Tian, J.M., Cheng, H.C., and Zhang, H.B., Modification of the interface and its influence on the performance of W–6 wt % TiC composite, *Mater. Sci. Eng. A*, 2021, vol. 819, p. 141442.
https://doi.org/10.1016/j.msea.2021.141442
20. Wei, Y., Chen, Y., Guo, B., and Zhu, L., The microstructure and mechanical properties of TiC-reinforced W-matrix composites prepared by spark plasma sintering, *Int. J. Refract. Met. Hard Mater.*, 2023, vol. 112, p. 106158.
https://doi.org/10.1016/j.ijrmhm.2023.106158
21. Ghazanfari, H., Blais, C., Alamdari, H., Gariepy, M., and Schulz, R., Mechanically activated combustion synthesis of Fe_3Al composite powders reinforced with sub-micrometer TiC particles, *J. Alloys Compd.*, 2018, vol. 761, pp. 71–79.
https://doi.org/10.1016/j.jallcom.2018.05.145
22. Lengauer, W., Transition metal carbides, nitrides, and carbonitrides, *Handbook of Ceramic Hard Materials*, Riedel, R., Ed., Wiley-VCH Publisher, 2000, pp. 202–252.
https://doi.org/10.1002/9783527618217.ch7
23. Lee, J., Jang, K., Lee, S., Mo, C.B., Kim, H., Park, K.R., Kim, J., Bang, J., Jung, I.C., Kim, J.C., and Mhin, S., Mechanical properties of TiC reinforced MgO–ZrO_2 composites via spark plasma sintering, *Ceram. Int.*, 2023, vol. 49, pp. 17255–17260.
https://doi.org/10.1016/j.ceramint.2023.02.091
24. Testa, V., Morelli, S., Bolelli, G., Bosi, F., Puddu, P., Colella, A., Manfredini, T., and Lusvarghi, L., Corrosion and wear performances of alternative TiC-based thermal spray coatings, *Surf. Coat. Technol.*, 2022, vol. 438, p. 128400.
https://doi.org/10.1016/j.surfcoat.2022.128400
25. Wang, X., Yang, Y., Zhao, Y., Zhang, X., Wang, Y., and Tian, W., Effects of B_4C particle size and content on microstructure and properties of in-situ TiB_2–TiC composite coatings prepared by plasma spraying, *Surf. Coat. Technol.*, 2023, vol. 459, p. 129273.
https://doi.org/10.1016/j.surfcoat.2023.129273
26. Vallauri, D., Atias Adrian, I.C., and Chrysanthou, A., TiC–TiB_2 composites: A review of phase relationships, processing and properties, *J. Eur. Ceram. Soc.*, 2008, vol. 28, no. 8, pp. 1697–1713.
https://doi.org/10.1016/j.jeurceramsoc.2007.11.011
27. Rahimi-Vahedi, A., Adeli, M., and Saghafian, H., Formation of Fe–TiC composite clad layers on steel using the combustion synthesis process, *Surf. Coat. Technol.*, 2018, vol. 347, pp. 217–224.
https://doi.org/10.1016/j.surfcoat.2018.04.086
28. Lemboub, S., Boudebane, S., Gotor, F.J., Haouli, S., Mazrag, S., Bouhedja, S., Hesser, G., Chadli, H., and Chouchane, T., Core-rim structure formation in TiC–Ni based cermets fabricated by a combined thermal explosion/hot-pressing process, *Int. J. Refract. Met. Hard Mater.*, 2018, vol. 70, pp. 84–92.
https://doi.org/10.1016/j.ijrmhm.2017.09.014
29. Zhang, F., Shi, F.-J., Dong, B.-X., and Yang, H.-Y., Effect of Ta, Nb and Zr additions on the microstructures and mechanical properties of 70 vol % TiC/Al cermets, *Ceram. Int.*, 2022, vol. 48, pp. 32479–32490.
https://doi.org/10.1016/j.ceramint.2022.07.194
30. Zhao, H., Li, J., Guo, S., Fan, D., Liu, G., and Li, J., Fast preparation of ZTA–TiC–FeCrNi cermets by high-gravity combustion synthesis, *Ceram. Int.*, 2017, vol. 43, pp. 6904–6909.
https://doi.org/10.1016/j.ceramint.2017.02.112
31. Gibot, P. Oudot, F., Lallemand, B., Schnell, F., and Spitzer, D., Nanosized niobium (V) and tantalum (V)

oxide ceramics as competitive oxidizers within aluminium-based nanothermites, *Energ. Mater. Front.*, 2021, vol. 2, pp. 167–173.
https://doi.org/10.1016/j.enmf.2021.07.001

32. Miloserdov, P.A., Gorshkov, V.A., Andreev, D.E., Yukhvid, V.I., Miloserdova, O.M., and Golosova, O.A., Metallothermic SHS of Al_2O_3–Cr_2O_3 + TiC ceramic composite material, *Ceram. Int.*, 2023, vol. 49, pp. 24071–24076.
https://doi.org/10.1016/j.ceramint.2023.04.145
33. Munir, Z.A. and Anselmi-Tamburini, U., Self-propagating exothermic reactions: The synthesis of high-temperature materials by combustion, *Mater. Sci. Rep.*, 1989, vol. 3, pp. 277–365.
https://doi.org/10.1016/0920-2307(89)90001-7
34. Zarezadeh Mehrizi, M., Beygi, R., Mostaan, H., Raoufi, M., and Barati, A., Mechanical activation-assisted combustion synthesis of in situ aluminum matrix hybrid (TiC/Al_2O_3) nanocomposite, *Ceram. Int.*, 2016, vol. 42, pp. 17089–17094.
https://doi.org/10.1016/j.ceramint.2016.07.219
35. Hu, Q., Luo, P., and yan, Y., Microstructures, densification and mechanical properties of TiC–Al_2O_3–Al composite by field-activated combustion synthesis, *Mater. Sci. Eng. A*, 20085, vol. 486, pp. 215–221.
https://doi.org/10.1016/j.msea.2007.08.075
36. Sharifitabar, M., Vahdati Khaki, J., and Haddad Sabzevar, M., Formation mechanism of TiC–Al_2O_3–Fe_3Al composites during self-propagating high-temperature synthesis of TiO_2–Al–C–Fe system, *Ceram. Int.*, 2016, vol. 42, pp. 12361–12370.
https://doi.org/10.1016/j.ceramint.2016.05.009
37. Ahmed, Y.M.Z., Zaki, Z.I., Besisa, D.H.A., Amin, A.M.M., and Bordia, R.K., Effect of zirconia and iron on the mechanical properties of Al_2O_3/TiC composites processed using combined self-propagating synthesis and direct consolidation technique, *Mater. Sci. Eng. A*, 2017, vol. 696, pp. 182–189.
https://doi.org/10.1016/j.msea.2017.04.059
38. Xia, W. and Mehrizi, M.Z., Direct synthesis of NiAl intermetallic matrix composite with TiC and Al_2O_3 reinforcements by mechanical alloying of NiO–Al–Ti–C powder mixture, *Ceram. Int.*, 2021, vol. 47, pp. 26863–26868.
https://doi.org/10.1016/j.ceramint.2021.06.095
39. Ali-Rachedi, M., Ramdane, W., Vrel, D., Benaldjia, A., Langlois, P., and Guerioune, M., The role of sintering additives on synthesis of cermets by auto-combustion, *Powder Technol.*, 2010, vol. 197, pp. 303–308.
https://doi.org/10.1016/j.powtec.2009.10.009
40. Niyomwas, S., Synthesis and characterization of TiC and TiC–Al_2O_3 composite from wood dust by self-propagating high temperature synthesis, *Energy Procedia*, 2011, vol. 9, pp. 522–531.
https://doi.org/10.1016/j.egypro.2011.09.060
41. Vrel, D., Hendaoui, A., and Andasmas, M., Synthesis of Ti–Al–C MAX phases byaluminothermic reduction process, *MAX Phases: Microstructure, Properties and Applications*, Low, I.-M. and Zhou, Y., Eds., Nova Science Publisher, 2012, pp. 29–51.
42. Benaldjia, A., Guellati, O., Bounour, W., Guerioune, M., Ali-Rachedi, M., Amara, A., Drici, A., and Vrel, D., Titanium carbide by the SHS process ignited with aluminothermic reaction, *Int. J. Self-Propag. High-Temp. Synth.*, 2008, vol. 17, no. 1, pp. 54–57.
https://doi.org/10.3103/S1061386208010068
43. Zhang, G., Yang, X., Zhao, Y., Yang, Z., and Li, J., Microstructure and mechanical properties regulation and control of in-situ TiC reinforced $CoCrFeNiAl_{0.2}$ high-entropy alloy matrix composites via high-gravity combustion route, *J. Alloys Compd.*, 2022, vol. 899, p. 163221.
https://doi.org/10.1016/j.jallcom.2021.163221
44. Saidi, A., Chrysanthou, A., Wood, J.V., and Kellie, J.L.F., Characteristics of the combustion synthesis of TiC and Fe–TiC composites, *J. Mater. Sci.*, 1994, vol. 29, pp. 4993–4998.
https://doi.org/10.1007/BF01151089
45. Yang, Y.F., Wang, H.Y., Zhao, R.Y., Liang, Y.H., Zhan, L., and Jiang, Q.C., Effects of C particle size on the ignition and combustion characteristics of the SHS reaction in the 20 wt % Ni–Ti–C system, *J. Alloys Compd.*, 2008, vol. 460, pp. 276–282.
https://doi.org/10.1016/j.jallcom.2007.06.010
46. Yang, Y.F. and Jiang, Q.C., Reaction behaviour, microstructure and mechanical properties of TiC–TiB_2/Ni composite fabricated by pressure assisted self-propagating high-temperature synthesis in air and vacuum, *Mater. Des.*, 2013, vol. 49, pp. 123–129.
https://doi.org/10.1016/j.matdes.2013.02.036
47. Liang, Y., Han, Z., Lin, Z., and ren, L., Study on the reaction behavior of self-propagating high-temperature synthesis of TiC ceramic in the Cu–Ti–C system, *Int. J. Refract. Met. Hard Mater.*, 2012, vol. 35, pp. 221–227.
https://doi.org/10.1016/j.ijrmhm.2012.06.002
48. Yen, C.L. and Sung W.Y., Combustion synthesis of Ni_3Al intermetallic compound in self-propagating mode, *J. Alloys Compd.*, 2004, vol. 384, pp. 181–191.
https://doi.org/10.1016/j.jallcom.2004.04.116
49. Yen, C.L., Ke, C.Y., Combustion synthesis of FeAl–Al_2O_3 composites with TiB_2 and TiC additions via metallothermic reduction of Fe_2O_3 and TiO_2, *Trans. Nonferrous Met. Soc.*, 2020, vol. 30, pp. 2510–2517.
https://doi.org/10.1016/S1003-6326(20)65397-3
50. Riyadi, T.W.B., Zhang, T., Marchant, D., and Zhu, X., NiAl–TiC–Al_2O_3 composite formed by self-propagation high temperature synthesis process: Combustion behaviour, microstructure, and properties, *J. Alloys Compd.*, 2019, vol. 805, pp. 104–112.
https://doi.org/10.1016/j.jallcom.2019.04.349
51. Pribytkov, G.A., Baranovskiy, A.V., Firsina, I.A., Korzhova, V.V., Krinitcyn, M.G., Korosteleva, E.N., Ti–TiC Composites by thermal explosion in mechanically activated Ti–xC powder blends (x = 1.0–6.3 wt %), *Int. J. Self-Propag. High-Temp. Synth.*, 2021, vol. 30, no. 2, pp. 87–93.
https://doi.org/10.3103/S1061386221020102
52. Bogatov, Yu.V. and Shcherbakov, V.A., TiC–20% Cr(Ni) composites by forced shs compaction: Influence of mechanical activation mode, *Int. J. Self-Propag. High-Temp. Synth.*, 2021, vol. 30, no. 1, pp. 58–59.
https://doi.org/10.3103/S1061386221010039
53. Seplyarskii, B.S., Abzalov, N.I., Kochetkov, R.A., and Lisina, T.G., Convection-Driven Combustion of (Ti + C) + xNi ($x \le 20$ wt %) granules in the absence of external gas flow, *Int. J. Self-Propag. High-Temp. Synth.*,

2020, vol. 29, no. 4, pp. 237–239.
https://doi.org/10.3103/S1061386220040123

54. Novikov, N.P., Borovinskaya, I.P., and Merzhanov, A.G., *Combustion Processes in Chemical Technology and Metallurgy*, Chernogolovka, 1975.
55. Song, M.S., Huang, B., Zhang, M.X., and Li, J.G., Study of formation behavior of TiC ceramic obtained by self-propagating high-temperature synthesis from Al–Ti–C elemental powders, *Int. J. Refract. Met. Hard Mater.*, 2009, vol. 27, pp. 584–589.
https://doi.org/10.1016/j.ijrmhm.2008.09.009
56. Zou, B., Xu, J., Wang, Y.,Zhao, S., Fan, X., Hui, Y., Zhou, X., Huang, W., Cai, X., Tao, S., Ma, H., and Cao, X., Self-propagating high-temperature synthesis of TiC–TiB_2-based Co cermets from a Co–Ti–B_4C system and fabrication of coatings using the cermet powders, *Chem. Eng. J.*, 2013, vol. 233, pp. 138–148.
https://doi.org/10.1016/j.cej.2013.07.125
57. Seplyarskii, B.S., Kochetkov, R.A., and Abzalov, N.I., SHS of TiC–Ni composites from powdered and granulated (Ti + C) + *x*Ni mixtures, *Int. J. Self-Propag. High-Temp. Synth.*, 2018, vol. 27, no. 3, pp. 189–191.
https://doi.org/10.3103/S1061386218030093
58. Yang, J., La, P., Liu, W., and Hao, Y., Microstructure and properties of Fe_3Al–$Fe_3AlC_{0.5}$ composites prepared by self-propagating high temperature synthesis casting, *Mater. Sci. Eng. A*, 2004, vol. 382, pp. 8–14.
https://doi.org/10.1016/j.msea.2004.03.095
59. Rogachev, A.S., Vadchenko, S.G., Kochetov, N.A., Kovalev, D.Yu., Kovalev, I.D., Shchukin, A.S., Gryadunov, A.N., Baras, F., and Politano, O., Combustion synthesis of TiC-based ceramic-metal composites with high entropy alloy binder, *J. Eur. Ceram. Soc.*, 2020, vol. 40, pp. 2527–2532.
https://doi.org/10.1016/j.jeurceramsoc.2019.11.059
60. Bowen, C.R. and Derby, B., Finite-difference modelling of self-propagating high temperature synthesis of materials, *Acta Metall. Mater.*, 1995, vol. 43, pp. 3903–3913.
https://doi.org/10.1016/0956-7151(95)90173-6
61. Rezaeezadeh, M., Shafiee Afarani, M., and Sharifitabar, M., WC–TiC–Al_2O_3 composite powder preparation by self-propagating high-temperature synthesis route, *Ceram. Int.*, 2017, vol. 43, pp. 15685–15693.
https://doi.org/10.1016/j.ceramint.2017.08.128
62. Bao, Y., Huang, L., An, Q., Jiang, S., Zhang, R., Geng, L., and Ma, X., Insights into arc-assisted self-propagating high temperature synthesis of TiB_2–TiC ceramic coating via wire-arc deposition, *J. Eur. Ceram. Soc.*, 2020, vol. 40, pp. 4381–4395.
https://doi.org/10.1016/j.jeurceramsoc.2020.05.005
63. Ahmed, Y.M.Z., Zaki, Z.I., Bordia, R.K., Besisa, D.H.A., and Amin, A.M.M., Simultaneous synthesis and sintering of TiC/Al_2O_3 composite via self propagating synthesis with direct consolidation technique, *Ceram. Int.*, 2016, vol. 42, pp. 16589–16597.
https://doi.org/10.1016/j.ceramint.2016.07.080
64. Choi, Y. and Rhee, S.W., Reaction of TiO_2–Al–C in the combustion of TiC–Al_2O_3 composite, *J. Am. Ceram. Soc.*, 1995, vol. 78, pp. 986–992.
https://doi.org/10.1111/j.1151-2916.1995.tb08426.x
65. Kim, J.W., Lee, J.M., Lee, J.H., and Lee, J.C., Role of excess Al on the combustion reaction in the Al–TiO_2–C system, *Met. Mater. Int.*, 2014, vol. 20, pp. 1151–1156.
https://doi.org/10.1007/s12540-014-6020-8
66. Chen, C.C., Phase equilibria at Ti–Al interface under low oxygen pressure, *Atlas J. Mater. Sci.*, 2014, vol. 1, pp. 1–11.
https://doi.org/10.5147/ajms.v1i1.116
67. Mostaan, H., Mehrizi, M.Z., Rafiei, M., Beygi, R., and Abbasian, A.R., Contribution of mechanical activation and annealing in the formation of nanopowders of Al(Cu)/TiC–Al_2O_3 hybrid nanocomposite, *Ceram. Int.*, 2017, vol. 43, pp. 2680–2685.
https://doi.org/10.1016/j.ceramint.2016.11.082
68. Mehrizi, M.Z. and Mofrad, S.S., Synthesis of NiAl/TiC–Al_2O_3 composite by mechanically activated combustion synthesis, *Ceram. Int.*, 2021, vol. 47, pp. 9258–9263.
https://doi.org/10.1016/j.ceramint.2020.12.052
69. Liang, Y., Han, Z., Li, X., Zhang, Z., and Ren, L., Study on the reaction mechanism of self-propagating high-temperature synthesis of TiC in the Cu–Ti–C system, *Mater. Chem. Phys.*, 2012, vol. 137, pp. 200–206.
https://doi.org/10.1016/j.matchemphys.2012.09.007
70. Xia, T.D., Munir, Z.A., Tang, Y.L., Zhao, W.J., and Wang, T.M., Structure formation in the combustion synthesis of Al_2O_3–TiC composites, *J. Am. Ceram. Soc.*, 2000, vol. 83, pp. 507–512.
https://doi.org/10.1111/j.1151-2916.2000.tb01225.x
71. Cho, C.H. and Kim, D.K., Microstructure evolution and isothermal compaction in TiO_2–Al–C combustion reaction, *J. Mater. Synth. Process.*, 2002, vol. 10, pp. 127–134.
https://doi.org/10.1023/A:1021934529088
72. Shen, P., Zou, B., Jin, S., and Jiang, Q., Reaction mechanism in self-propagating high temperature synthesis of TiC–TiB_2/Al composites from an Al–Ti–B_4C system, *Mater. Sci. Eng. A*, 2007, vol. 454, pp. 300–309.
https://doi.org/10.1016/j.msea.2006.11.055
73. Biswas, A., Roy, S.K., Gurumurthy, K.R., Prabhu, N., and Banerjee, S., A study of self-propagating high-temperature synthesis of NiAl in thermal explosion mode, *Acta Mater.*, 2002, vol. 50, no. 4, pp. 757–773.
https://doi.org/10.1016/S1359-6454(01)00387-1
74. Gedevanishvili, S. and Deevi, S.C., Processing of iron aluminides by pressureless sintering through Fe–Al elemental route, *Mater. Sci. Eng. A*, 2002, vol. 325, no. 1, pp. 163–176.
https://doi.org/10.1016/S0921-5093(01)01442-3
75. Li, Y.X., Hu, J.D., Wang, H.Y., and Guo, Z.X., Dissolution-precipitation mechanism of laser igniting self propagating high-temperature synthesis of Al/TiC composite, *Adv. Eng. Mater.*, 2007, vol. 9, no. 8, pp. 689–694.
https://doi.org/10.1002/adem.200700088
76. Holt, J. and Munir, Z., Combustion synthesis of titanium carbide: theory and experiment, *J. Mater. Sci.*, 1986, vol. 21, no. 1, pp. 251–259.
https://doi.org/10.1007/BF01144729
77. Kubaschewsky, O., *Materials Thermochemistry*, Pergamon Press, 1993.
78. Mossino, P., Some aspects in self-propagating high-temperature synthesis, *Ceram. Int.*, 2004, vol. 30, no. 3, pp. 311–332.
https://doi.org/10.1016/S0272-8842(03)00119-6

79. Sharifi, E.M., Karimzadeh, F., and Enayati, M.H., Mechanochemically synthesized Al_2O_3–TiC nanocomposite, *J. Alloys Compd.*, 2010, vol. 491, nos. 1–2, pp. 411–415. https://doi.org/10.1016/j.jallcom.2009.10.206

80. Moore, J.J. and Feng, H.J., Combustion synthesis of advanced materials: Part II. Classification, applications and modelling, *Prog. Mater. Sci.*, 1995, vol. 39, pp. 275–316. https://doi.org/10.1016/0079-6425(94)00012-3

81. Laloy, J., Lozano, O., Alpan, L., Mejia, J., Toussaint, O., Masereel, B., Dogné, J.-M., and Lucas, S., Can TiC nanoparticles produce toxicity in oral administration to rats?, *Toxicol Rep.*, 2014, vol. 1, pp. 172–187. https://doi.org/10.1016/j.toxrep.2014.03.004

82. Hoseini, S.M.H., Adeli, M., Hoseini, S.A., and Hoseini, S.A., Solution combustion synthesis of Mg–TiC@NiO nanocomposite and investigation on its metallurgical and biological properties, *J. Mol. Liq.*, 2023, vol. 376, p. 121487. https://doi.org/10.1016/j.molliq.2023.121487

83. Li, S.-S., Zhang, H., Chang, F., Fei, Y.-N., Kou, S.-Q., Shao, Y., Xuan, Q.-Q., Li, X., and Qiu, F., Effects of alloy elements (Mg, Zn) on the microstructure and mechanical properties of (TiC + TiB_2)/Al composites, *Ceram. Int.*, 2022, vol. 48, pp. 22096–22105. https://doi.org/10.1016/j.ceramint.2022.04.201

84. Huang, X., Zhang, L., Zhao, Z., and Yin, C., Microstructure transformation and mechanical properties of TiC–TiB_2 ceramics prepared by combustion synthesis in high gravity field, *Mater. Sci. Eng. A*, 2012, vol. 553, pp. 105– 111. https://doi.org/10.1016/j.msea.2012.05.099

85. Courtney, T.H., *Mechanical Behavior of Materials*, New York: McGraw-Hill Education, 1990.

86. Qiu, F., Zuo, R., Shu, S., and Wang, Y.-W., Effect of Al addition on the microstructures and compression properties of (TiC_xN_y–TiB_2)/Ni composites fabricated by combustion synthesis and hot press, *Powder Technol.*, 2015, vol. 286, pp. 716–721. https://doi.org/10.1016/j.powtec.2015.09.016